Injectable thermosensitive antibiotic-laden chitosan hydrogel for regenerative endodontics

Alexandre Henrique dos Reis-Prado [a,b], Maedeh Rahimnejad [a], Renan Dal-Fabbro [a],
Priscila Toninatto Alves de Toledo [a,c], Caroline Anselmi [a,d],
Pedro Henrique Chaves de Oliveira [a,c], J. Christopher Fenno [e],
Luciano Tavares Angelo Cintra [c], Francine Benetti [b],
Marco C. Bottino [a,f,*]

[a] Department of Cariology, Restorative Sciences and Endodontics, University of Michigan School of Dentistry, Ann Arbor, MI, USA
[b] Department of Restorative Dentistry, Universidade Federal de Minas Gerais (UFMG), School of Dentistry, Belo Horizonte, MG, Brazil
[c] Department of Preventive and Restorative Dentistry, School of Dentistry, São Paulo State University (UNESP), Araçatuba, SP, Brazil
[d] Department of Morphology and Pediatric Dentistry, São Paulo State University (UNESP) - Araraquara School of Dentistry, Araraquara, SP, Brazil
[e] Department of Biologic and Materials Sciences & Prosthodontics, University of Michigan School of Dentistry, Ann Arbor, MI, USA
[f] Department of Biomedical Engineering, College of Engineering, University of Michigan, Ann Arbor, MI, USA

ARTICLE INFO

ABSTRACT

Injectable biomaterials, such as thermosensitive chitosan (CH)-based hydrogels, present a highly translational potential in dentistry due to their minimally invasive application, adaptability to irregular defects/shapes, and ability to carry therapeutic drugs. This work explores the incorporation of azithromycin (AZI) into thermosensitive CH hydrogels for use as an intracanal medication in regenerative endodontic procedures (REPs). The morphological and chemical characteristics of the hydrogel were assessed by scanning electron microscopy (SEM), energy dispersive spectroscopy (EDS), and Fourier transform infrared spectroscopy (FTIR). The thermosensitivity, gelation kinetics, compressive strength, cytocompatibility, and antibacterial efficacy were evaluated according to well-established protocols. An *in vivo* model of periapical disease and evoked bleeding in rats' immature permanent teeth was performed to determine disinfection, tissue repair, and root formation. AZI was successfully incorporated into interconnected porous CH hydrogels, which retained their thermosensitivity. The mechanical and rheological findings indicated that adding AZI did not adversely affect the hydrogels' strength and injectability. Incorporating 3 % and 5 % AZI into the hydrogels led to minimal cytotoxic effects compared to higher concentrations while enhancing the antibacterial response against endodontic bacteria. AZI-laden hydrogel significantly decreased *E. faecalis* biofilm compared to the controls. Regarding tissue response, the 3 % AZI-laden hydrogel improved mineralized tissue formation and vascularization compared to untreated teeth and those treated with double antibiotic paste. Our findings demonstrate that adding 3 % AZI into CH hydrogels ablates infection and supports neotissue formation *in vivo* when applied to a clinically relevant model of regenerative endodontics.

1. Introduction

Conventional endodontic treatment of immature permanent teeth with pulp necrosis remains challenging due to the thin and fragile dentin walls, which increase the risk of root fractures [1]. The open apex may also lead to the extrusion of filling materials, further complicating the treatment [1]. Regenerative endodontics procedures (REPs) are biologically based therapies for necrotic immature permanent teeth, founded on the three pillars of tissue engineering: bioactive molecules, stem cells, and three-dimensional scaffolds. This clinical therapy seeks to physiologically substitute or restore impaired tooth structures and cells of the pulp-dentin complex, thereby enhancing the longevity of the tooth

and reinstating its functionality [2,3]. However, residual bacterial infection promotes a constant inflammatory stimulus, affecting the development of remaining dentin and consequently impairing the regenerative outcome [4].

Triple or double antibiotic pastes are some intracanal medications preferred for REPs among endodontics and pediatric dentists [5]. However, alternative disinfection strategies are being actively explored to overcome the drawbacks associated with these medications, with a growing emphasis on cell-friendly strategies to eradicate bacterial infection within the root system while supporting successful tissue regeneration [6]. After ensuring infection ablation, the following clinical step involves inducing bleeding through over-instrumentation to fill the root canal space with periapical blood. This procedure allows a significant influx of stem cells from the periapical tissues. The resulting blood clot, enriched with cells and bioactive molecules released during dentin matrix conditioning, acts as a natural scaffold, playing a role in stem cell homing and tissue repair [7,8].

Injectable gels represent an innovative type of hydrogel network characterized by their fluidity, which allows for minimally invasive application into small areas such as the root canal [9]. Thermosensitive injectable hydrogels maintain a liquid state at specific temperatures and transition into gels upon injection into the body. These hydrogels are designed to undergo reversible sol-gel transformations under physiological conditions (37 °C), possessing mechanical properties comparable to living tissues [9]. Among these thermosensitive materials, chitosan (CH), when combined with weak bases including beta-glycerol phosphate (BGP) and sodium hydrogen carbonate (SHC), emerges as a prominent class of thermosensitive polymers [10,11]. Chitosan-based injectable hydrogels, responsive to temperature and pH changes, offer multiple advantages: they can absorb significant amounts of water, are minimally invasive, and form porous structures that adapt well to irregularly shaped defects. Additionally, it can be integrated with antibiotics and other biologically active compounds, increasing its therapeutic potential.

Azithromycin (AZI) belongs to the second-generation macrolide class of antibiotics. It effectively targets a broad spectrum of aerobic and anaerobic gram-positive and gram-negative bacteria and is noted for its improved pharmacokinetic properties [12]. Structurally, AZI is a semi-synthetic, acid-stable molecule characterized by a 15-membered azlactone ring [13]. Notably, a study highlighted azithromycin's capacity to modulate macrophage polarization from pro-inflammatory (M1) to pro-resolving (M2) states in induced periapical lesions in mice [11], facilitating the resolution of periapical inflammation, underscoring AZI's accompanying immunomodulatory effects [14].

Although clinical studies have demonstrated that REPs can enhance root maturation and promote periapical healing when properly performed [15–17], literature on regenerative endodontics indicates that the newly formed tissues in REPs predominantly represent repair rather than true regeneration [15,18]. Consequently, more histological studies are necessary to ensure predictable clinical outcomes for REPs and to elucidate the nature of the newly formed tissues in immature teeth with apical periodontitis following these procedures, particularly through microbial control using more cell-friendly disinfecting strategies [15,19]. While some animal studies have suggested that chitosan scaffolds do not significantly enhance mineralized tissue formation compared to evoked bleeding alone [18,20], none has explored the *in vivo* regenerative potential of a thermosensitive chitosan formulation used as an intracanal medication in a necrotic animal tooth model. Furthermore, given AZI's promising ability to resolve periapical inflammation through infection control and its immunomodulatory effects, its combination with this chitosan hydrogel shows potential for improving regenerative outcomes.

In this work, distinct concentrations of AZI were incorporated into thermosensitive chitosan hydrogels for use as an intracanal medication in regenerative endodontics. Here, the hydrogels' morphological structure, pore diameter, and chemical composition were characterized using scanning electron microscopy (SEM) and Fourier-transform infrared (FTIR) spectroscopy. To determine the impact of AZI addition on the thermosensitivity, gelation kinetics was evaluated through rheology, followed by a mechanical evaluation to assess the compressive properties of the hydrogels. The AZI-laden CH hydrogels' cytocompatibility, antibacterial efficacy against endodontic bacteria, *E. faecalis* biofilm inhibition, and release profile were also assessed. A well-established *in vivo* model of periapical disease in rodents was performed to examine the clinical potential of the formulated AZI-laden hydrogels on periapical lesion ablation and its combinatorial effect, along with evoked bleeding on continued root development, inflammatory profile, and angiogenesis.

2. Materials and methods

2.1. Preparation of azithromycin-laden chitosan hydrogels

Firstly, for the preparation of the CH solution, 50 mL of 0.12 M hydrochloric acid (HCl; Fisher Scientific, Nazareth, PA, USA) was prepared in a beaker by mixing 44 mL of Milli-Q water with 6 mL of 1 M HCl [10]. The beaker was then placed under a motor stirrer set to stir slowly. Gradually, 1.665 g of chitosan powder (Sigma-Aldrich, St. Louis, MO, USA) was added into the 50 mL of 0.12 M HCl while stirring at 700–800 rpm for 2–3 h. Once the CH powder was fully dissolved, the mixture was transferred into an appropriate bottle. Finally, the solution was autoclaved at 121 °C for 20 min.

To obtain 1 mL of the CH hydrogel, 0.6 mL of the CH solution was mixed with 0.2 mL of gelling agent containing 0.5 M β-glycerophosphate disodium salt hydrate (BGP; Sigma-Aldrich, St. Louis, MO, USA) and 0.075 M sodium hydrogen-carbonate (SHC; EMSURE®, Darmstadt, Germany) as reported by Assad et al. [10]. Then, this solution was mixed with 0.2 phosphate-buffered solution (PBS; Gibco™, Thermo Fisher Scientific, Waltham, MA, USA). For the mixing procedures, 3 mL syringes containing each of the three solutions connected by a Luer-lock connector were used, as shown in Supplementary File 1. For the preparation of the CH-modified hydrogel supplemented with Azithromycin, AZI powder (TCI AMERICA, Portland, OR, USA) was weighed based on the desired concentrations (vol/wt ratio; 3 %, 5 %, 10 %, 15 %, and 25 %), added into the 0.2 mL of PBS, vortexed, and mixed with the other CH/gelling agent solution as described above (Supplementary File 2).

2.2. Morphological and chemical analyses

Morphological characterization of the fabricated hydrogels supplemented or not with AZI (3 % and 5 %) was carried out using a scanning electron microscope (SEM, MIRA3, FEG-SEM, TESCAN Brno, Kohoutovice, Czech Republic). Energy dispersive X-ray spectroscopy (EDS) was performed to analyze the chemical composition. The samples were frozen for 14 days, freeze-dried, and coated with Au-Pd by sputtering. For chemical analysis, Fourier transformed infrared (FTIR) spectroscopy (16 scans with wavelength range from 4000 to 400 cm^{-1} at 2 cm^{-1} resolution) in the Attenuated Total Reflectance mode (ATR-FTIR, Thermo-Nicolet iS-50, Thermo Fisher Scientific Inc., Waltham, MA, USA) was performed using a PerkinElmer instrument (PerkinElmer Inc., Waltham, MA, USA) to assess the presence of AZI in the CH hydrogel. FTIR spectra were baseline-corrected and normalized for analysis.

2.3. Rheological properties

The rheological properties of the hydrogels were studied using a TA-instrument rheometer equipped with 20-mm parallel plates (PP) geometry. Immediately following the preparation of each hydrogel, amplitude sweep was investigated as a function of strain (0.01–100 %) to determine linear viscoelastic region (LVE). To study gelation kinetics, the variation with time of storage modulus (G′) and loss modulus (G″) was measured in the linear viscoelastic range at a constant strain (0.01

%) and a constant frequency (1 Hz). The measurements were conducted at 22 °C (room temperature, RT) for 10 min, followed by 37 °C (body temperature) for 10 min. The viscosity behavior of the pre-hydrogel solutions at 22 °C was assessed using rotational rheometric tests using the previously reported strategy for time- and temperature-dependent hydrogels [21]. Briefly, the viscosity was studied as a function of time at different shear rates (10, 100, 500 s^{-1}). To express the shear-thinning behavior, the viscosity values at specific time points were plotted as a shear rate function. A time point of 10 min was chosen, assuming this corresponds to the time required for hydrogel preparation and injection. To study the recovery properties after injection, the oscillatory test was performed, including pre-injection (0.01 % strain, 5 min, 22 °C), injection (100 % strain, 1 min, 22 °C), and post-injection (0.01 % strain, 5 min, 37 °C). In addition, a record demonstrating the injection of 1 mL CH hydrogel can be seen in Supplementary File 3.

2.4. Mechanical properties

To evaluate the impact of the AZI incorporation in the compressive properties (strain, stress, maximum stress, and Young's modulus) of CH hydrogel, cylindrical-shaped samples (10 mm diameter × 5 mm thick) were prepared for all tested groups. Before evaluation, the samples (n = 6/group) were incubated in a distilled water bath for 24 h at 37 °C and dried using low-lint paper. Mechanical testing was performed at RT at a strain rate of 2 mm/min (expert 5601, ADMET, Inc., Norwood, MA, USA).

2.5. Cytocompatibility

To investigate whether CH hydrogel and different concentrations (3–25%) of AZI-laden CH hydrogels would lead to cytotoxicity on stem cells of the apical papilla (SCAPs), samples of hydrogels (8 mm diameter × 3 mm thick) were prepared following the International Standards Organization guidelines (ISO10993-5: tests for cytotoxicity—*in vitro* methods). SCAPs were cultivated in an incubator at 37 °C, with 5 % CO$_2$ in α-MEM supplemented with 15 % of fetal bovine serum (FBS; Gibco, Carlsbad, CA, USA) and 1 % of antibiotic solution (Penicillin-Streptomycin 10,000 U/mL; Gibco, Carlsbad, CA, USA). Cells at passages 4–7 were used.

Six hydrogel samples per group were first UV-treated for 30 min on each side for disinfection and then individually placed in sterile glass vials containing 5 mL of α-MEM supplemented with 10 % FBS, l-glutamine, 1 % penicillin-streptomycin, and 1 U/mL of collagenase type I. Then, samples were incubated at 37 °C at predetermined time points (1, 3, 7, 14, and 21 days), and 500 μL aliquots were collected at the predetermined time points to determine the cytotoxicity over time. Of note, the same volume of fresh media was added back to each vial to keep the extraction volume constant. The collected aliquots were filtered through a 0.22 μm membrane (Corning syringe filters; New York, NY, USA) before being applied to the cells [22].

SCAPs were seeded on 96-well cell-culture plates (1 × 10^4 cells/well). After 24 h, the medium was replaced by 100 μL extracts from the hydrogels and kept in contact with the cells for 24 h. Cells treated with α-MEM medium without FBS were used as a negative control group. In contrast, cells treated with 0.3 % phenol red (Sigma-Aldrich, St. Louis, MO, USA) were used as a positive control for toxicity. Subsequently, cells were exposed to 100 μL of 10 % alamarBlue (Invitrogen, Carlsbad, CA, USA) in α-MEM without FBS for 3 h at 37 °C and 5 % CO$_2$. Fluorescence intensity was measured at 560 nm excitation and 590 nm emission. Cell viability was calculated by converting fluorescence values into percentages, with the negative control at each time point set as 100 %.

2.6. Antibacterial properties

The antibacterial properties of all formulated hydrogels (3–25 % AZI) were tested against endodontic-related infection bacteria using agar diffusion and biofilm inhibition assays.

2.6.1. Direct and indirect contact assays

Six samples per group were used for the direct contact agar diffusion assay. Hydrogels were prepared and stored in sterile conditions in 1.5 mL Eppendorf. Three endodontic-related microorganisms were tested: *Enterococcus faecalis* (*Ef*, ATCC 19433), *Actinomyces naeslundii* (*An*, ATCC 12104), and *Fusobacterium nucleatum* (*Fn*, ATCC 25586) [13]. *Ef* was cultured aerobically at 37 °C in normal atmosphere. On the other hand, *An* and *Fn* were cultured at 37 °C in an anaerobic chamber (5 % CO$_2$, 10 % hydrogen, 85 % N$_2$), all in 5 mL of non-supplemented BHI (Brain Heart Infusion, Sigma-Aldrich, St. Louis, MO, USA) broth for 24 h. The bacterial suspension was standardized to approximately 3 × 10^8 colony-forming units (CFU)/mL, with optical density (OD) at 600 nm as a reference. Subsequently, 100 μL of each target bacterial broth was spread onto agar plates to create a bacterial lawn, and then the sterile blank disks were placed. The agar plates were divided into 4 zones: three for the 50 μL CH-based samples and one for the positive control with 10 μL of 0.12 % chlorhexidine (CHX; Sigma-Aldrich, St. Louis, MO, USA) in distilled water. The negative control was the CH group. BHI agar plates (Sigma-Aldrich, St. Louis, MO, USA) were used for *Ef* and incubated at 37 °C in normal atmosphere for 24 h. For *An* and *Fn*, Brucella Agar plates with Hemin and Vitamin K1 (Sigma-Aldrich, St. Louis, MO, USA), containing 5 % sheep blood (Defibrinated, Thermo Fisher Scientific, Waltham, MA, USA), were used and incubated at 37 °C for 48 h in an anaerobic chamber. After incubation, the diameters of the inhibition halos were measured in millimeters and reported as mean ± SD [23].

For the indirect assay, cylindrical-shaped samples (8 mm diameter × 3 mm thick) were prepared from each group (n = 3), disinfected with UV light for 30 min on each side, and individually placed in sterile glass vials containing 5 mL of PBS. The samples were incubated at 37 °C at predetermined time points (1, 3, 7, 14, and 21 days). At each time point, 500 μL aliquots were collected from the vials to assess antibacterial activity over time, with 500 μL of fresh PBS replacing the collected aliquots. The collected aliquots were stored at −20 °C and filtered through a 0.22 μm membrane (Corning syringe filters; New York, NY, USA) before use. *Ef* was grown, and 100 μL was spread onto Brain-Heart-Infusion (BHI) agar plates to form a bacterial lawn. Sterile blank disks (Thermo Fisher Scientific, Waltham, MA, USA) were placed on the agar, and 20 μL of the aliquots collected at each time point were added to the disks. Additionally, 20 μL of CHX 0.12 % was used as a positive control. The negative control was the CH group. The plates were incubated at 37 °C in a normal atmosphere. The plates were incubated, and the inhibition zone was assessed as previously described.

2.6.2. Mature biofilm formation

The antibiofilm properties of CH-based hydrogels were assessed in an *Ef* mature biofilm assay on dentin slices. For this, newly extracted, caries-free third molars were collected at the Community Dental Center (University of Michigan, Ann Arbor, MI, USA) with the donor's consent and approval by the institutional review board (IRB: HUM00154490). Teeth were cleaned and preserved in 0.01 % sodium azide (Sigma-Aldrich). The crowns were sectioned using the Isomet 1000 Precision Saw (Buehler, Waukegan Rd, IL, USA) to produce dentin slices 700 μm thick. The slices were then standardized for surface roughness by polishing with 600-grit grinding paper under water cooling and disinfected by immersion in 2.5 % sodium hypochlorite (NaOCl) and 17 % ethylenediaminetetraacetic acid (EDTA) solution in an ultrasonic bath for 5 min each. After rinsing with PBS (Gibco™, Thermo Fisher Scientific, Waltham, MA, USA) for 10 min, the slices were autoclaved at 121 °C for 20 min. The sterilized dentin slices were placed aseptically in 24-well culture plates (Corning, New York, NY, USA), and 1.8 mL of BHI broth containing 1 % sucrose (Sigma-Aldrich, St. Louis, MO, USA) was added to each sample, followed by 200 μL of a spectrophotometrically adjusted 7.5 × 10^8 CFU/mL *Ef* suspension.

The plates were incubated at 37 °C with 5 % CO_2 for 7 days, with media refreshed every 48 h. After this period, 50 μL of CH-based hydrogels containing pure CH, 3 %, and 5 % AZI were applied to the top of the dentin slices. The plates were then incubated with PBS for another 7 days at 37 °C with 5 % CO_2, with media refreshed every 48 h. Untreated dentin samples and those treated with double antibiotic paste (DAP; 5 mg/mL and 50 mg/mL metronidazole/ciprofloxacin, Sigma-Aldrich, St. Louis, MO, USA) served as negative and positive controls, respectively. To simulate the clinical setting, DAP was used as a positive control in accordance with the clinical recommendations of the American Association of Endodontists [24]. CFU (n = 6) was assessed by dislodging the biofilm using sonication (25 W for 10 s), followed by 30 s vortexing, serial dilutions, and plating the bacteria onto BHI agar plates. The plates were incubated at 37 °C in a normal atmosphere for 24 h, and CFU was counted for each group. The remaining 2 samples per group were prepared for SEM analysis to qualitatively examine the biofilm on the dentin slices at 10000 × and 20000 × magnification (scale bar of 10 μm).

2.7. In vivo infected immature permanent teeth model of periapical disease

Eighteen male 4-week-old Fisher 344 rats (~80 g) were used (Envigo RMS, Inc., Oxford, MI, USA), following the ARRIVE (Animal Research: Reporting of *In Vivo* Experiments) guidelines for reporting animal research and were per the regulations of the local institutional Animal Care and Use Committee (PRO00010911). The animals were kept in mini-isolators, three animals/cage, and received solid food and water "ad libitum," with environment and light cycle control (22 ± 1 °C, 70 % humidity at 12 h light and 12 h dark). The procedures were performed under general anesthesia induced with 50 mg/kg of Ketamine (Hospira, Inc., Lake Forest, IL, USA) and 5 mg/kg of xylazine (Akorn, Inc.; Lake Forest, IL, USA) via intraperitoneal. The sample size was calculated based on a previous study of rats with induced periapical inflammation submitted to REPs [25]. The calculation was based on the Statistical Package for Sigma Plot (version 12.0; Systat Software Inc., Palo Alto, CA, USA). It was considered a 95 % power and alpha-type error level of 0.05, having 5 M as a sample size per group. Considering the mortality that could have occurred, one more molar was added in each group, totalizing 6 M per group following previous studies [3,25,26]. With four groups in total, 24 M were required.

2.7.1. Surgical procedures

The upper right and left immature first molar of the animals were randomly allocated into four groups (n = 6/group): Health tooth (HT), Necrosis (N), 50 mg/mL double antibiotic paste (1:1 metronidazole and ciprofloxacin) (50 mg/mL DAP) and CH Hydrogel + 3 % AZI (CH + 3 % AZI). All surgical procedures were performed by a single calibrated and experienced operator using a dental microscope (Evolution XR6, Seiler, St. Louis, Missouri, USA). Initially, the teeth were isolated with a gingival barrier (FMG, Fort Lauderdale, Florida, USA). Then, endodontic access in the mesial root canal was performed with a ½ dental round burr (Kavo Kerr Group, Charlotte, NC, USA) under consistent irrigation with saline solution. The teeth remained open for 21 days to induce a periapical lesion [27,28]. After this period, the protocol for disinfection was performed. Firstly, using 29G NaviTip™ tips (length of 17 mm; Ultradent Products, Inc., South Jordan, UT, USA), the mesial root canals were irrigated with 2.5 % NaOCl for 5 min with constant renovation and aspiration of the solution. Subsequently, irrigation with 17 % EDTA (0.1 mL/min) for 5 min was carried out [3,15]. A saline solution was applied after the irrigation with each solution to promote their complete removal. Subsequently, the root canals were dried with sterile paper points (Absorbent paper points, DENTSPLY Maillefer, Tulsa, OK, USA) and medicated with the different intracanal medications, 50 mg/mL DAP (clinical reference, positive control) or CH+3%AZI (formulated hydrogel). The medications were delivered using a 1 mL disposable luer

slip syringe (Descarpack, São Paulo, SP, Brazil) and 25G blunt needles (0.012″ × 0.30 mm, 1.000″; Lexington, KY, USA), with 0.01 mL placed inside the mesial root canal. After the AZI-laden hydrogel crosslinked due to the temperature increase within the mesial root canal, the cavity was sealed with glass ionomer restorative material (Ketac Molar, 3M Science, Seefeld, Bavaria, Germany). Fourteen days later, teeth were re-entered, and the irrigation was performed only with 17 % EDTA for 5 min. Afterward, the same drying protocol was done. Based on the clinically approved protocol, intracanal bleeding (Evoked bleeding technique) was induced by a #10 K-file (DENTSPLY Maillefer, Tulsa, OK, USA) at 0.5 mm beyond the foramen, using a counterclockwise push-and-pull motion until the root canals were filled with blood from the periapical tissues [3,26]. Finally, MTA Angelus® White (Angelus®, Londrina, PR, Brazil) reparative cement was placed for the coronal barrier, and the cavities were sealed with glass ionomer restorative material (Ketac Molar, 3M Science, Seefeld, Bavaria, Germany). For postoperative analgesia, the rats received a single subcutaneous dose of dipyrone at 150 mg/kg (Neo Química; São Paulo, SP, Brazil). Daily monitoring was performed using the Rat Grimace Scale, a partially automated method for quantifying pain in laboratory rats by analyzing facial expressions. Twenty-eight days later, the animals were euthanized, and the samples were retrieved for analysis.

2.7.2. Micro-computed tomography (μCT)

A non-destructive examination of root development and the reduction of periapical lesions was conducted using a Scanco μCT 100 (Scanco Medical AG, Wangen-Brüttisellen, Zurich, Switzerland). The scanning parameters included 70 kV, 114 μA monochromatic x-rays, and voxel sizes of 12 μm. The exposure time was averaged to 3 frames per 500 ms. The Scanco Medical System software facilitated the image reconstruction process. The resulting 3D images were utilized to trace the initial defects circumferentially, designating these areas as the regions of interest (ROI). Each specimen's ROI was analyzed for root length, root thickness, and periapical lesion volume.

In sagittal views, the length of the mesial root was measured by drawing a line from the apex to the center of the upper margin of the root. The thickness was assessed at three specific locations: the cervical side at the upper quarter (cervical 1/4), the central portion at the midhalf (central 1/2), and the apical side at the lower quarter (apical 1/4) of the root. To evaluate the periradicular lesion volume, a ROI was delineated around the root and apical foramen, beginning from the first transaxial slice showing bone resorption, extending through the apex, and concluding at the final slice where normal bone structure reappeared. Each measurement was conducted three times for each sample, and the average of these measurements was calculated and utilized for analysis.

2.7.3. Histological and immunofluorescence analyses

Following the μCT scan, the samples underwent a four-week decalcification process in 10 % EDTA and subsequently embedded in paraffin. Serial histological sections, 5-μm thick, were prepared by cutting the samples in the mesiosagittal plane. Sections were selected from the point where the mesial root of the first molar was fully visible along its longitudinal axis, yielding seven slides per sample. The first slide was stained with hematoxylin and eosin (H&E), followed by Masson's trichrome (MT) and Brown and Breen (B&B). The slides were analyzed once by a single calibrated and blinded operator to the groups using a brightfield microscope (Echo Revolve, BICO Company, San Diego, CA, USA) at 200 × . Images of the periapical region of the mesial root were obtained to visualize tissue organization, newly formed cementum, inflammatory reaction, collagen detection, and presence of microorganisms.

For immunofluorescence, sections were dewaxed at 60 °C for 15 min and rehydrated using ethanol gradients. To decrease endogenous peroxidase activity, the sections were incubated for 20 min in a 3 % hydrogen peroxide solution at RT. The slides were treated with a

background snipper solution for 20 min at RT to block nonspecific binding. Later, sections were incubated overnight at 4 °C with anti-inducible nitric oxide synthase (iNOS; dilution 1:100; rabbit recombinant multiclonal, ab283655, Abcam, Cambridge, MA, USA), anti-CD163 (dilution 1:100; rabbit monoclonal, ab182422, Abcam, Cambridge, MA, USA), anti-CD31/PECAM1 (dilution 1:100; rabbit monoclonal, 00055, Fortis Life Sciences, Waltham, MA, USA), and anti-osteopontin (dilution 1:100; rabbit polyclonal, ab216402, Abcam, Cambridge, MA, USA). This was followed by a 1-h incubation at RT with goat anti-rabbit IgG H&L (Alexa Fluor 568, ab175471, Abcam, Cambridge, MA, USA), goat anti-rabbit IgG H&L (Alexa Fluor 488, ab150077, Abcam, Cambridge, MA, USA) at dilution 1:100. Finally, the cell nuclei were stained using VECTASHIELD antifade mounting medium with DAPI (Vector Laboratories, Newark, CA, USA). Images were captured at $100 \times$ magnification in the apical region of the mesial root, using fluorescent filters using the Echo Revolve microscope (Discover Echo Inc., San Diego, CA, USA). The areas of positive immunofluorescence staining were quantified using ImageJ software (1.53v, National Institutes of Health). The process involved importing the images, splitting the channels to isolate the color corresponding to the secondary antibody, and adjusting the threshold values. The lower threshold was set to 100, and the upper threshold was set to 255 to reflect true positive immunolabeling accurately. Finally, the positive staining area was measured as a percentage of the total image area [24].

2.8. Statistical analysis

Statistical analysis was performed using GraphPad Prism software (Version 9.5.1; GraphPad Software, Inc., San Diego, CA). After assessing data distribution (Shapiro-Wilk test), non-parametric data, including pore diameter measurements, were evaluated using the Kruskal-Wallis test, followed by Dunn's. In contrast, parametric data, such as compression data, cytocompatibility, antibacterial activity, and *in vivo* results, were subjected to one-way or two-way analysis of variance (ANOVA) followed by Tukey's and Games-Howell's post-hoc tests, considering a significance level of $p < 0.05$.

3. Results

3.1. AZI-laden hydrogel displayed an interconnected porous structure

The bulk microstructure morphology and pore size of the pure and AZI-laden CH hydrogels were initially examined by SEM, as presented in Fig. 1. All formulations, with or without AZI, displayed a 3D porous network with interconnected pores. The AZI groups showed the presence of AZI particles on their surfaces (Fig. 1A). No variation in pore morphology was observed upon AZI incorporation. Regarding the frequency distribution, AZI-laden CH hydrogels showed a similar profile with a high frequency of 4000 nm $\pm$ 2326.9 pores for CH+3%AZI and 4000 nm $\pm$ 4000.8 for CH+5%AZI (approximately 30 %). In comparison, pure CH hydrogel (control) presented frequencies of 3000 nm $\pm$ 1577.1 pore diameters (approximately 28 %). A higher pore diameter was observed for both AZI-laden CH hydrogel groups (3 and 5 % AZI) than the CH hydrogel group (Fig. 1B).

Surface SEM images of pure CH hydrogels showed a homogeneous and smooth surface, while incorporation of AZI resulted in a rough beaded surface covered with AZI particles (Fig. 2A–C). These particles were also visible deep inside the chitosan matrix. EDS analysis revealed an increase in the intensity of carbon and oxygen with increasing AZI concentrations compared to pure CH hydrogel, confirming the
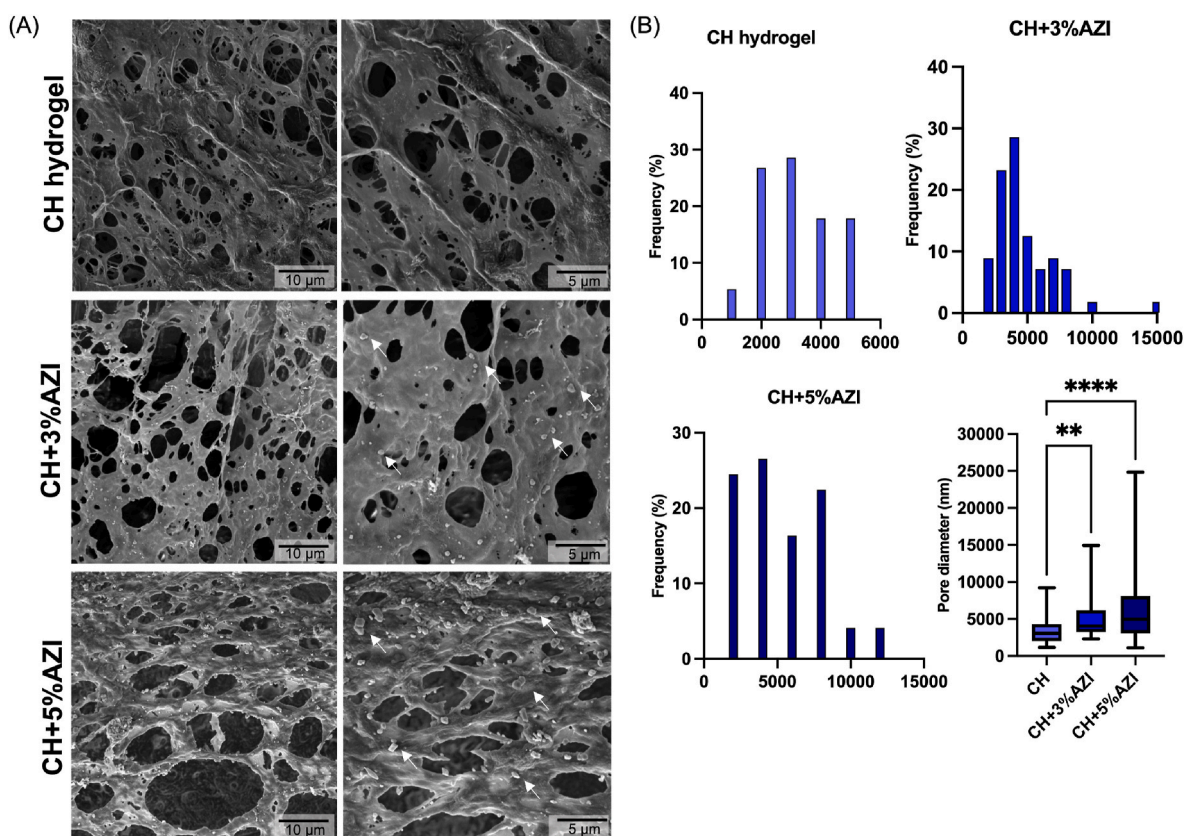

Fig. 1. Bulk microstructure morphological characterization of pure, 3 %, and 5 % AZI-laden CH hydrogels. (A) Scanning electron microscopy (SEM) images at magnification levels of $5000 \times$ and $10,000 \times$. White arrows indicate the presence of AZI particles; (B) Histograms show the frequency distribution (%) of pore diameters, and boxplots indicate the median values of pore diameters for all groups (25th–75th percentiles). *Asterisk indicates statistical differences between groups (Kruskal-Wallis and Dunn's tests; $**p < 0.01$, $****p < 0.0001$).
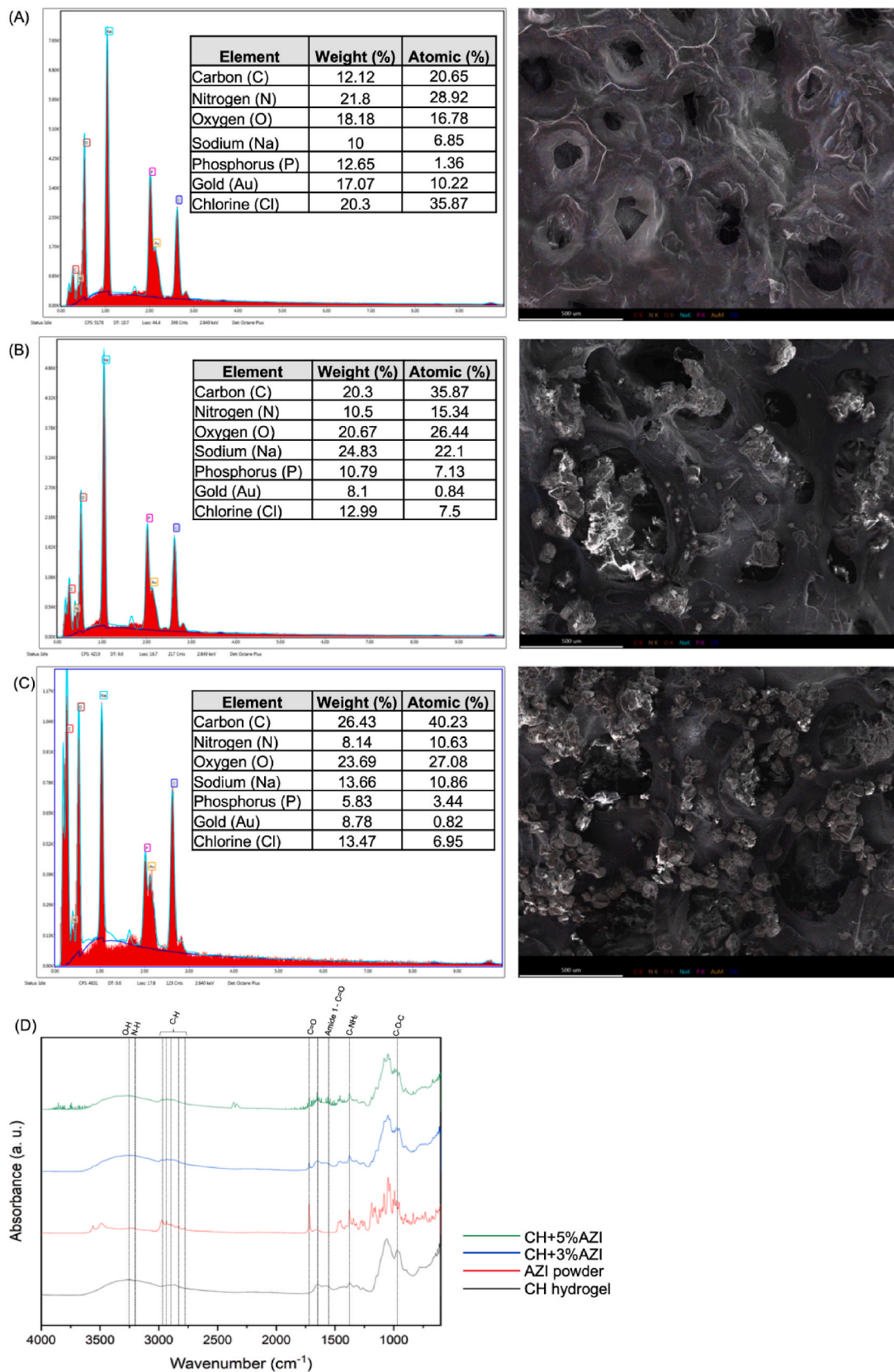
Fig. 2. Surface morphological and chemical characterization of pure, 3 %, and 5 % AZI-laden CH hydrogels. (A) Energy-dispersive x-ray spectroscopy profile (EDS) of chitosan (CH) hydrogel; (B) EDS of CH+3%AZI; (C) EDS of CH+5%AZI; and (D) Fourier-transform infrared spectroscopy spectra (FTIR) of pure CH hydrogels and incorporated with different concentrations of AZI.

successful AZI incorporation (Fig. 2A–C).

The FTIR spectra for the chitosan hydrogel (CH) and chitosan samples with different concentrations of azithromycin (AZI) are presented in Fig. 2D. Key characteristic peaks of AZI, marked by dashed vertical lines, appear at 3493.03, 1719.9, 1249.85, and 1082.15 cm^{-1}. These peaks correspond to the hydroxyl group, H-bonded OH, ketone carbonyl compounds, aromatic ethers, aryl -O stretch, and organic sulfates, respectively. Notably, these peaks are also observed in the CH + AZI samples' spectra, confirming AZI's presence in the chitosan matrix. Additional peaks in the AZI spectrum appear at 2907, 1720, 1363, 1190, 1108 cm^{-1}, and around 1350 cm^{-1}, which are associated with C-H (methyl group) stretching, C=O stretching, C=C bending, C-O-C asymmetrical stretching, C-O-C symmetrical stretching, and C-N stretching. These peaks are similarly reflected in the spectra of the CH + AZI samples, suggesting the successful incorporation of AZI within the chitosan structure. The consistent appearance of these characteristic AZI peaks in the AZI powder and the CH + AZI spectra indicates that the antibiotic's structural integrity is retained after incorporation.

The spectra of the CH hydrogels without AZI incorporation displayed the characteristic bands of the gelling agent used in preparing the thermosensitive hydrogels. Multiple intense bands attributed to phosphate groups were observed between 1400 and 800 cm^{-1}. Additionally, BGP exhibited a broad band between 3600 and 2800 cm^{-1} corresponding to hydroxyl and alkyl groups and intense bands between 1160 and 920 cm^{-1} ascribed to phosphate groups. However, the bands corresponding to SHC at 1700–1600 cm^{-1} and 1400–1300 cm^{-1} showed negligible intensity, likely due to the decomposition of SHC after mixing with the acidic CH solution.

3.2. AZI incorporation maintains thermosensitivity, mechanical integrity, and hydrogel injectability

The rheological properties of the hydrogels were assessed to determine the impact of AZI incorporation on their thermosensitivity and injectability. The linear viscoelastic (LVE) range, where the hydrogel's moduli G′ (storage modulus) and G″ (loss modulus) are independent of the applied strain, was determined using a strain sweep test with the strain amplitude set at 100 %. Fig. 3A shows the LVE range for each formulation, presenting the storage modulus (G′) and loss modulus (G″) as functions of strain. This test helps assess the hydrogels' mechanical behavior by evaluating how their stiffness (represented by G′) and viscoelasticity (represented by G″) change under strain. The storage modulus, G′, reflects the hydrogel's strength, with higher G′ values indicating greater material rigidity. While all hydrogels displayed a similar stiffness range, the addition of AZI and its increasing concentration caused a noticeable reduction in the LVE region, suggesting a decrease in the material's elastic behavior as more AZI was incorporated.

Time sweeps were conducted in the LVE region, initially at RT (22 °C) to evaluate the stability of the hydrogels before injection based on their composition, and subsequently at 37 °C to assess their gelation kinetics (solidification) upon in situ injection (Fig. 3B). The figure illustrates the evolution of G′ and G″ as a function of time. A significant increase in the G′ value during isothermal conditions at 37 °C indicates gel thermosensitivity and thermos-crosslinking. This thermosensitivity was most pronounced in the pure CH hydrogel. Conversely, increasing AZI concentration enhanced stability at RT and reduced thermosensitivity post-injection. Time sweep analysis also enabled the investigation
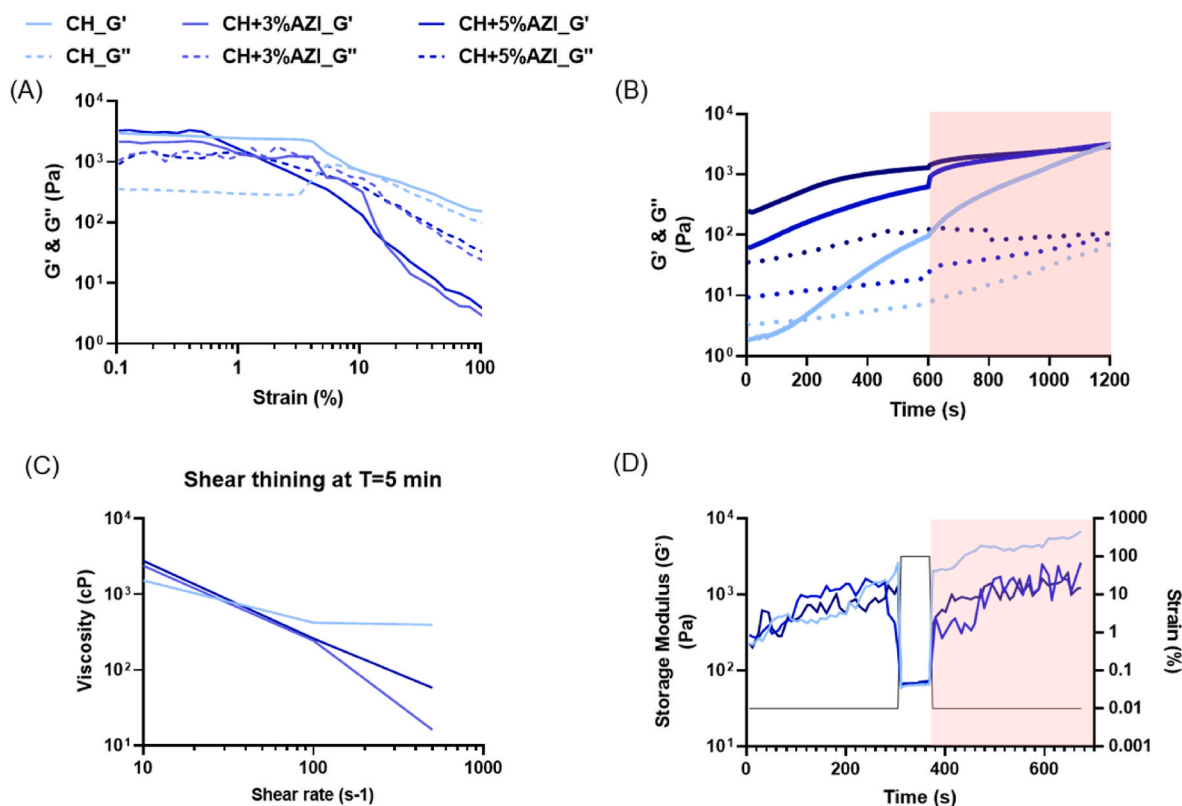

Fig. 3. Rheological characterization of pure, 3 %, and 5 % AZI-laden CH hydrogels: (A) Amplitude sweep showing the impact of AZI incorporation on linear viscoelastic (LVE) region of CH hydrogels (evolution of the storage (G′) and loss (G″) moduli, mean ± SD; n ⩾ 3); (B) Gelation kinetics of hydrogels, presenting the evolution of the storage (G′) as a function of time at 22 °C for 10 min and subsequently at 37 °C for 10 min (mean ± SD; n ⩾ 3); (C) Shear-thinning behavior of hydrogels as a function of shear rate after 5 min at 22 °C, studying viscosity profile at various shear rates (10, 100, and 500 s^{-1}) as a function of time (mean; n ⩾ 3); and (D) Recovery properties after before and injection: the graphs present the complete cycle, namely at-rest state (0.01 % strain, for 5 min), injection step (100 % strain for 1 min), post-injected rest state at 37 °C (strain back to 0.01 % for 5 min) (red zone refers to 37 °C) (mean ± SD; n ⩾ 3).

of gelation temperatures. The hydrogels transition to a viscoelastic gel when $G' > G''$. Following the approach of Winter and Chambon [29], gelation time is defined as the point where G' equals G'', or where the loss factor $\tan \delta = G''/G'$ equals 1. Gelation occurs rapidly for all formulations, typically within 15 s for AZI-laden hydrogels, as evidenced by G' exceeding G'' right from the initial measurement.

The shear-thinning property, essential for the injectability of hydrogels, is shown in Fig. 3C. All formulations exhibit shear-thinning properties, as evidenced by a significant drop in viscosity with increasing shear rate; however, notable differences exist between them, with AZI incorporation enhancing the degree of shear-thinning.

Following the schematic presented in Fig. 3D, to evaluate the hydrogel's ability to recover after injection, the recovery tests were conducted by monitoring the evolution of the storage modulus (G') during a stress condition. Initially, the hydrogels were rested at a strain of 0.01 %, followed by the application of 100 % strain for 1 min. After this deformation step, the strain was removed, and the recovery of G' was tracked over time at 37 °C, simulating the in-situ injection process. This procedure allows for assessing the material's ability to regain its original stiffness after undergoing high strain, reflecting its potential for restoring mechanical integrity post-injection. Consistent with previous findings, G' increased over time at rest, followed by a sharp decrease during injection due to shear thinning. Recovery immediately after strain removal was only partial when AZI was incorporated. However, all formulations returned to their initial G' values after 5 min.

The mechanical properties of the hydrogels before and after injection through a 25G-long needle were analyzed using compression tests (Fig. 4). Overall, the incorporation of 3 % AZI reduced the yield strain. However, no significant differences were observed before and after injection or between the groups. The ultimate strength showed a slight improvement with 3 % AZI incorporation, while a similar trend was observed between pure CH hydrogel and CH-5% AZI, with no significant differences, as demonstrated in Fig. 4C. The Young's modulus of the hydrogels exhibited consistency across all groups, both before and after injection, and between different formulations, as shown in Fig. 4D.

3.3. Lower antibiotic concentrations of AZI-laden hydrogels showed reduced cytotoxicity

A decrease in cell viability was identified for all AZI-laden CH groups compared to the negative control (untreated cells) ($p < 0.05$), as shown in Fig. 5. Cell viability levels higher than 70 % were observed only for the pure CH group at all the time points assessed. Although the incorporation of AZI decreased cell viability compared to the negative control and pure CH, there was a reduction in cytotoxic effects for the CH hydrogel loaded with 3 % and 5 % AZI compared to the other concentrations at days 14 and 21 ($p < 0.05$).

3.4. AZI enhanced the antibacterial activity of CH hydrogels against endodontic bacteria

The antibacterial results of the direct contact assay, as assessed by the agar diffusion method, are displayed in Fig. 6A. The mean zones of inhibition observed against the evaluated bacterial strains are presented in Tables 1, 2, and 3. Hydrogels containing 3 % and 5 % AZI exhibited larger inhibition zones than 0.12 % CHX and pure CH against *Ef* (Table 1), *An* (Table 2), and *Fn* (Table 3) ($p < 0.05$). No significant differences were observed between the AZI-laden hydrogels ($p > 0.05$).

In the indirect contact assay (Fig. 6B), all groups demonstrated sustained antimicrobial properties, with the most effective results observed in eluates from higher concentrations of AZI-laden CH hydrogels (15 % and 25 %) ($p < 0.05$). No significant differences were found between these higher-concentration AZI groups and the 0.12 % CHX group ($p > 0.05$). Most AZI-laden hydrogels exhibited superior antimicrobial performance against *Ef* compared to pure CH, particularly in the early time points (up to 7 days).

3.5. CH hydrogels containing 3 % and 5 % AZI eliminate biofilm as the clinical control

Regarding the mature biofilm model, the designed scaffolds' antibacterial effects were assessed quantitatively (Fig. 7A) and qualitatively (Fig. 7B). The quantitative data demonstrated that CH hydrogel containing 3 % and 5 % AZI significantly decreased *Ef* biofilm compared to the negative control (untreated), 5 mg/mL DAP paste, and pure CH ($p < 0.05$). There were no significant differences in the levels of CFU/mL between the groups containing AZI and 50 mg/mL DAP paste ($p > 0.05$). These results were confirmed by SEM imaging, which revealed fewer *Ef* bacterial cells/biofilm on the surface of the dentin discs treated with 50 mg/mL DAP paste and the AZI-laden CH hydrogels. Particles of AZI can be seen attached to the surface of bacterial membranes.

3.6. 3 % AZI-laden hydrogels encouraged root development and reduced periapical lesions in vivo

Regarding the µCT analysis, Fig. 8A shows 3D images of the first molar and the periapical lesion of the mesial root canal of rat molars in the sagittal, frontal, and transversal sections. The graphs depict statistical comparisons between groups for the evaluated outcomes (Fig. 8B).

The healthy tooth group exhibited a greater increase in root length compared to the Necrosis and CH+3%AZI groups. However, the difference between the healthy tooth and CH+3%AZI groups was less pronounced than the difference with the Necrosis group ($p < 0.05$). There was no significant difference in root length between the healthy tooth and the 50 mg/mL DAP groups ($p > 0.05$). Regarding root thickness, the healthy tooth group and the groups treated with the medications exhibited significantly greater thickness than the Necrosis group ($p < 0.05$). Regarding the volume of periapical lesions, a significant reduction was observed in the groups treated with 50 mg/mL DAP and CH+3%AZI compared to the Necrosis group ($p < 0.05$).

3.7. 3 % AZI-laden hydrogels controlled local infection and enhanced regenerative outcome

Twenty-eight days after REPs in the first upper immature molars of rats with pulp necrosis (Fig. 9), H&E indicated that the 50 mg/mL DAP and CH+3 % AZI groups led to a more pronounced cementum-like tissue area with cells similar to cementoblasts and cementocytes. These groups also had the presence of inflammatory cells, blood vessel-like structures, and partial ingrowth of newly formed connective tissue with prominent areas of collagen, as shown in the MT staining. In contrast, the absence of newly formed cementum-like tissue, intense area of inflammatory cells with disorganized tissue, and necrosis were observed in the Necrosis group. Regarding B&B staining, an intense presence of bacteria was observed in the Necrosis group compared to the treated groups.

Representative immunofluorescent images of the iNOS(M1)-, CD163 (M2)-, CD31$^-$, and osteopontin (OPN)-positive cells for all the evaluated groups are shown in Fig. 10A, with quantitative analysis displayed in Fig. 10B. Regarding the M1 and M2 analysis, a higher number of M1-positive cells was observed in the Necrosis group than in the treated groups and the healthy control ($p < 0.05$). At the same time, 50 mg/mL DAP showed a significant expression of M2-positive cells in the apical third of the first molar compared to the other groups ($p < 0.05$). Regarding angiogenesis, the CH+3%AZI group had a significantly higher number of CD31-positive vessels than the 50 mg/mL DAP and the Necrosis groups ($p < 0.05$). A higher number of OPN-positive cells was observed in the treated groups compared to the controls ($p < 0.05$) and in the 50 mg/mL DAP group compared to the CH+3%AZI group ($p < 0.05$).

4. Discussion

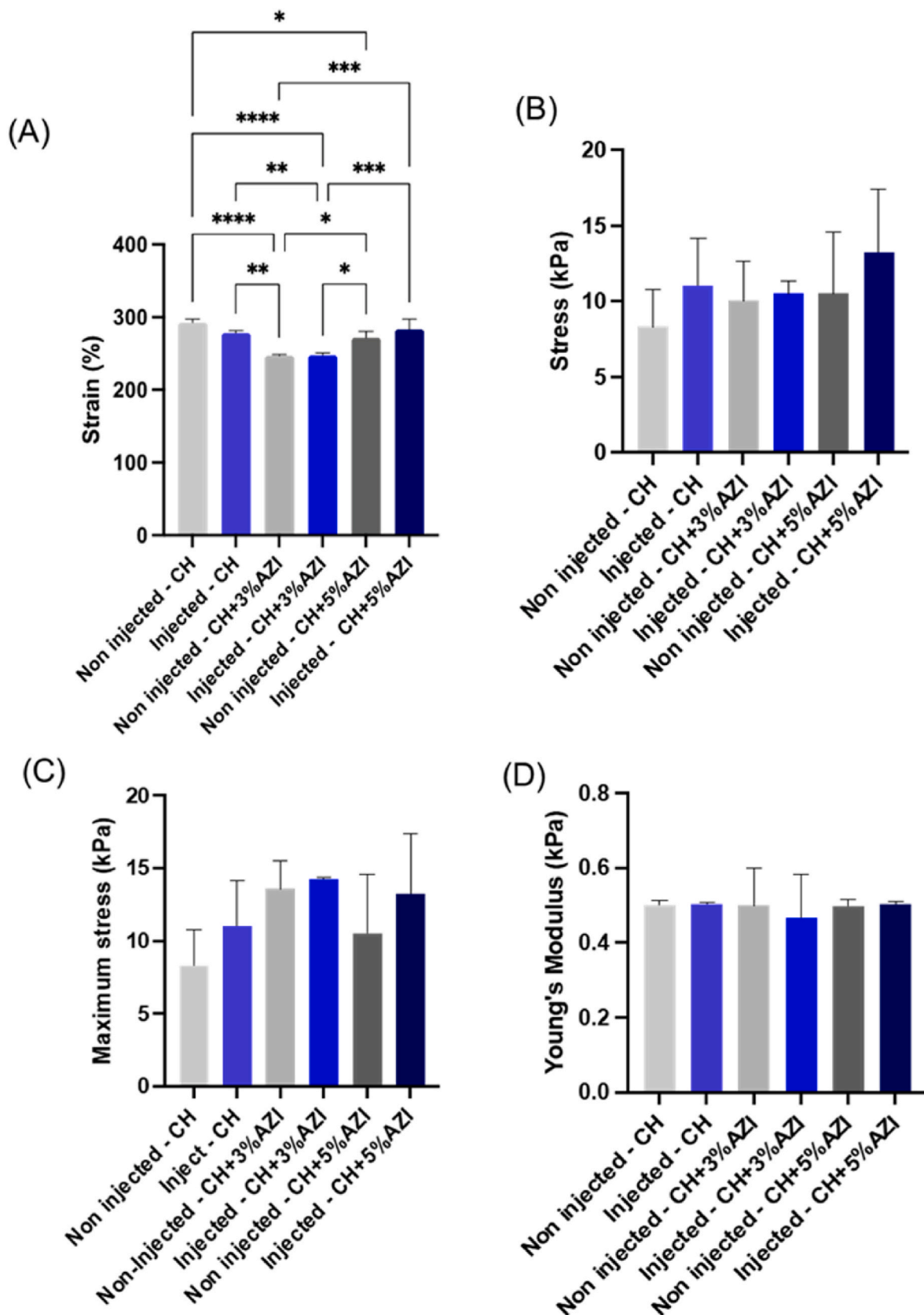Recently, a growing emphasis has been on developing novel drug

Fig. 4. Mechanical properties of pure, 3 %, and 5 % AZI-laden CH hydrogels before and after injection through a 25G long needle (0.012″ × 0.30 mm, 1.000″; Lexington, KY, USA): A) Yield Strain (%), B) Yield Stress (kPa), C) Maximum stress (Ultimate strength) (kPa), and D) Young's modulus (kPa) (mean ± SD, n = 6). *Asterisk indicates statistical differences between groups (One-way ANOVA followed by Tukey's test; *p < 0.05, **p < 0.01, ***p < 0.001, ****p < 0.0001).
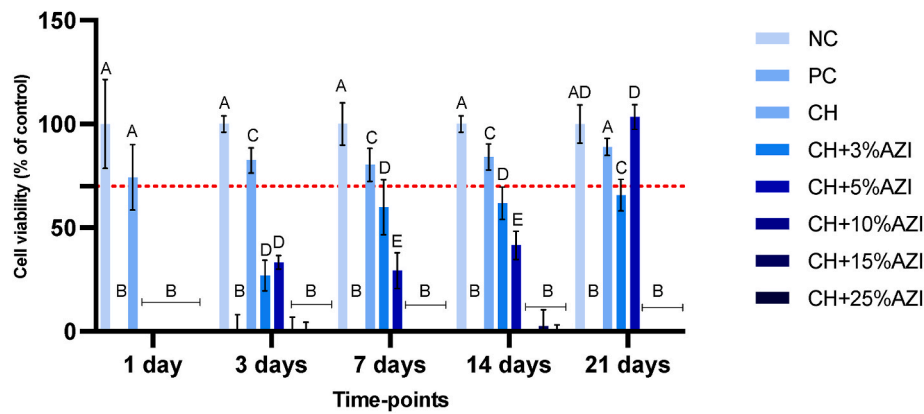
Fig. 5. Graphic representation of stem cells from the apical papilla (SCAPs) metabolic activity (% mean ± SD; AlamarBlue® assay) using aliquots collected at 1, 3, 7, 14, and 21 days. Fluorescence was measured at 560–590 nm. Different letters indicate significant differences between groups at each time point (one-way ANOVA followed by Tukey's or Games-Howell tests; $p < 0.05$). The horizontal red dashed line indicates the threshold of 70 % cell viability.
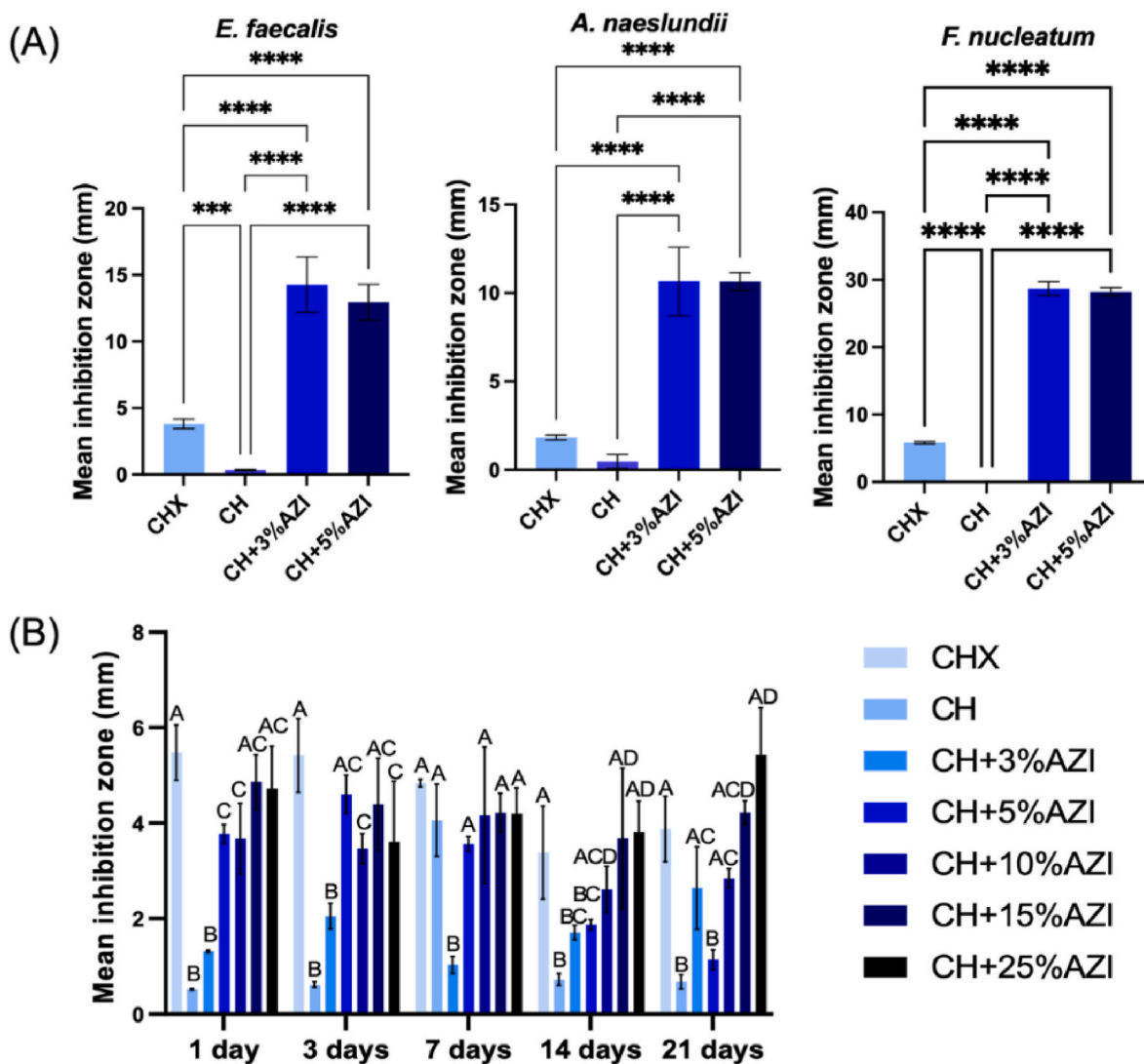

Fig. 6. Antibacterial activity of chitosan (CH) hydrogels and CH + AZI (3 % and 5 %). (A) Direct antibacterial activity (inhibition zones per mm) against *E. faecalis*, *A. naeslundii,* and *F. nucleatum* compared to chlorhexidine (CHX; positive control). Data is presented as mean ± SD (n = 6). *Asterisk indicates a significant difference between groups (one-way ANOVA followed by Tukey's test; ***$p < 0.001$, ****$p < 0.0001$). (B) Indirect antibacterial activity (inhibition zones) against *E. faecalis* compared to 0.12 % CHX as a positive control at 1, 3, 5, 7, 14, and 21 d. Data is presented as mean ± SD (n = 6). Different letters indicate significant differences between groups (two-way ANOVA followed by Tukey's test; $p < 0.05$).

Table 1
Zone of inhibition against *E. faecalis*.

Groups	Mean (mm)	SD	*P* value
0.12 % CHX	3.81	0.35	<0.001
CH	0.32	0.05	
CH+3%AZI	14.27	2.08	
CH+5%AZI	13.45	1.69	

One-way ANOVA followed by Tukey test, *P* > 0.05. AZI: azithromycin; CHX: chlorhexidine; CH: chitosan; SD: standard deviation.

Table 2
Zone of inhibition against *A. naeslundii*.

Groups	Mean (mm)	SD	*P* value
0.12 % CHX	1.83	0.12	<0.0001
CH	0.48	0.35	
CH+3%AZI	10.66	1.76	
CH+5%AZI	10.64	0.45	

One-way ANOVA followed by Tukey test, *P* > 0.05. AZI: azithromycin; CHX: chlorhexidine; CH: chitosan; SD: standard deviation.

Table 3
Zone of inhibition against *F. nucleatum*.

Groups	Mean (mm)	SD	*P* value
0.12 % CHX	5.82	0.17	<0.0001
CH	0.0	0.0	
CH+3%AZI	28.68	1.02	
CH+5%AZI	28.22	0.62	

One-way ANOVA followed by Tukey test, *P* > 0.05. AZI: azithromycin; CHX: chlorhexidine; CH: chitosan; SD: standard deviation.

delivery systems tailored for cell-friendly environments to enhance root canal disinfection during REPs without compromising stem cell differentiation and tissue regeneration [30]. This study focused on thermosensitive chitosan-based hydrogels incorporated with azithromycin (AZI), aiming to improve REPs outcomes and facilitate clinical application by enabling precise injection into root canals.

The thermosensitive injectable CH hydrogels were successfully formulated to incorporate AZI within interconnected porous structures, maintaining crucial mechanical, rheological, and injectability properties essential for clinical efficacy [31], which is in agreement with other researchers [21,32]. Rheology refers to the study of how materials deform and flow under applied forces, and it is particularly relevant in the context of injectable hydrogels because these materials must maintain specific characteristics to support cells effectively [11,21]. Firstly, injectable hydrogels must flow easily through a syringe needle during injection but quickly regain their gel-like state once injected to prevent dispersion from the target site. Secondly, the hydrogel's mechanical strength and viscoelastic properties are critical for maintaining structural integrity after injection. These properties dictate how well the hydrogel can support cell encapsulation and withstand physiological stresses *in vivo* [33]. Previous studies have established CH hydrogels as injectable biomaterials capable of supporting encapsulated cells [10, 11]. In this work, we have highlighted a positive outcome where the inclusion of 3 % AZI in CH formulations maintained viscoelastic properties. Despite observing adverse effects on thermosensitivity and post-injection recovery in other formulations with AZI, this particular combination with 3 % AZI demonstrated thermogelation at 37 °C, providing in-situ gelation after injection to the treating site, as well as shear thinning and fast recovery after injection. These findings underscore the delicate balance required when modifying CH hydrogel formulations with AZI to ensure that their essential properties, such as injectability and mechanical stability, are maintained or optimized without compromising efficacy.

The role of extracellular matrix (ECM) properties in determining the
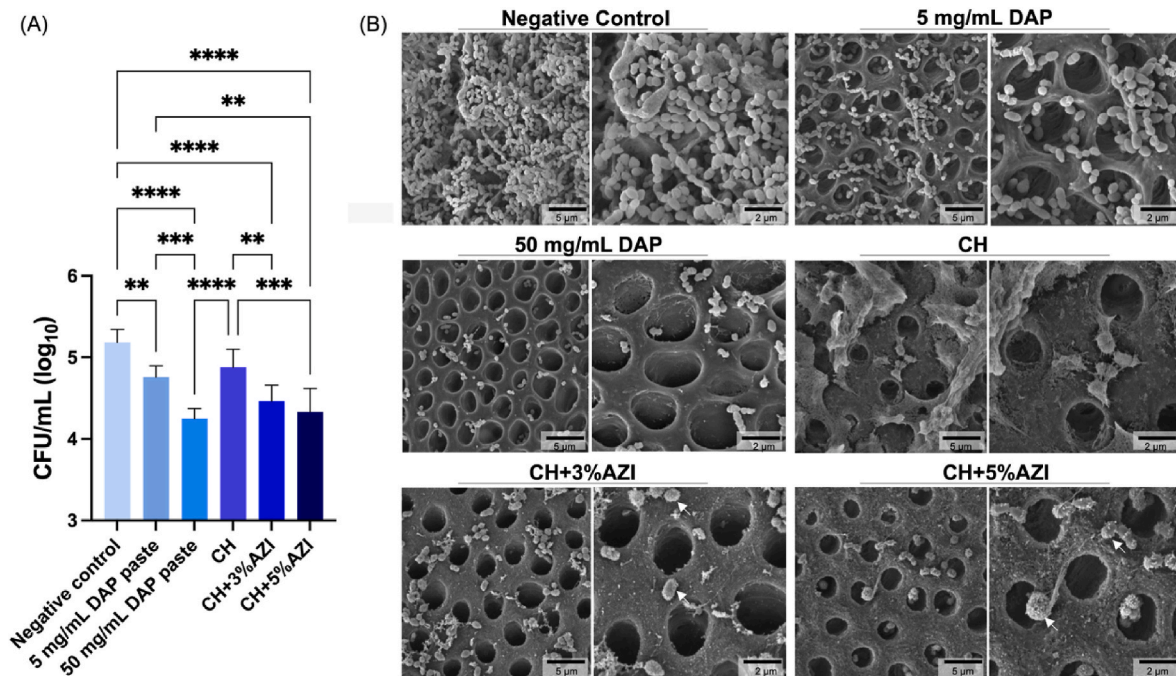

Fig. 7. Biofilm formation assay. (A) The number of *E. faecalis* cells ($\log_{10}$ CFU/mL) after 7 days of dentin biofilm exposure to chitosan (CH) and CH with AZI (3 % and 5 %) compared to double antibiotic paste (DAP) (positive control; metronidazole/ciprofloxacin). CH-based hydrogel loaded with 3 % and 5 % AZI significantly reduced bacterial numbers compared to all other groups ($p < 0.05$). The negative control was the original biofilm without any treatment. *Asterisk indicates significant difference between groups (one-way ANOVA followed by Tukey's test; **$p < 0.01$, ***$p < 0.001$, ****$p < 0.0001$)); (B) Scanning electron microscopy (SEM) images at 10,000 × and 20,000 × magnification of *E. faecalis* biofilm on the surface of dentin discs treated with CH, CH + AZI 3 % or CH + AZI 5 % for 7 days. White arrows indicate the particles of AZI attached to bacterial membranes.
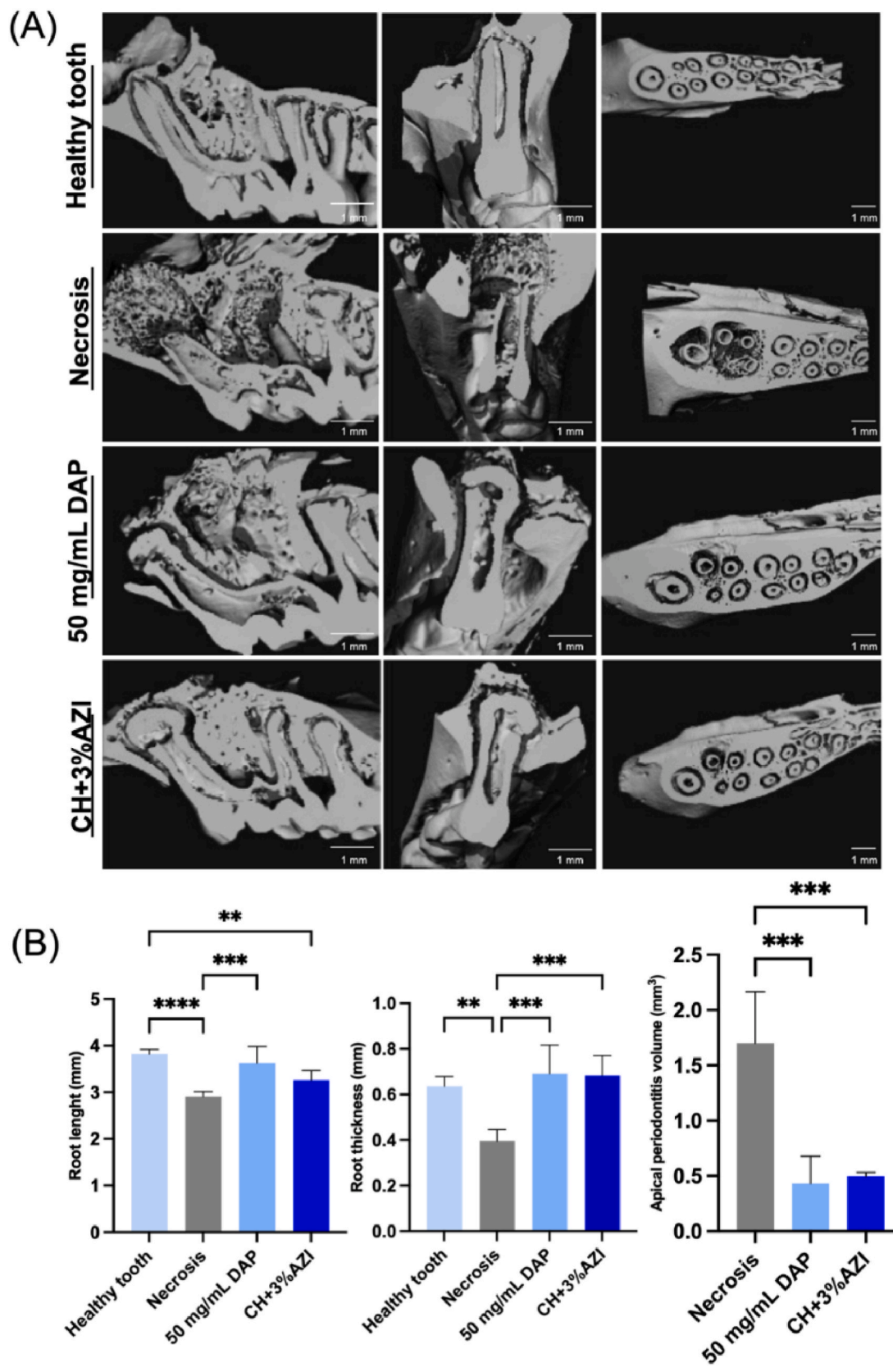
Fig. 8. (A) Representative 3D μCT images in the sagittal, frontal, and transversal sections of upper rat first molars. (B) Dentine length from the root tip to the crown, dentin thickness, and periapical lesion volume measured from mesial root canals of first rat molars. *Asterisk indicates significant differences between groups in each analysis (one-way ANOVA followed by Tukey's test; **$p < 0.05$, ***$p < 0.001$, ****$p < 0.0001$).
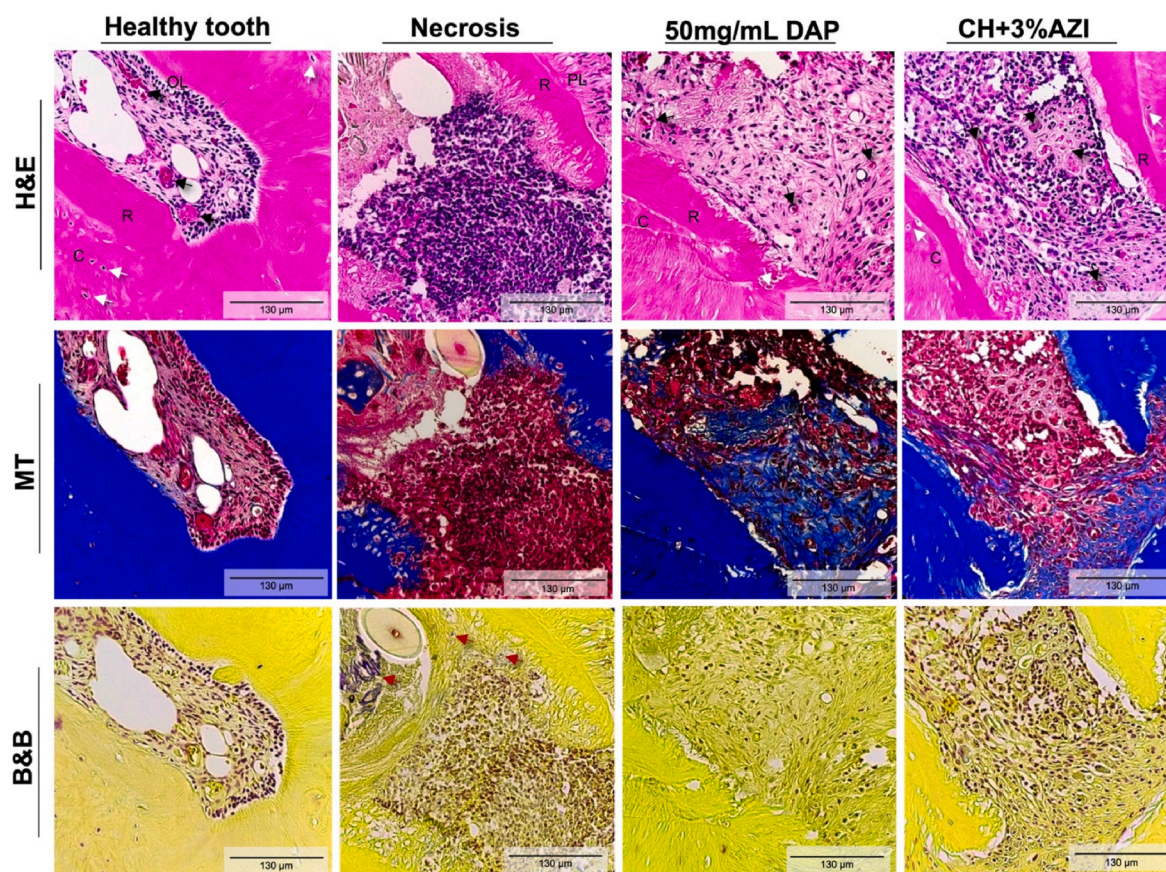
Fig. 9. Representative images of hematoxylin and eosin (H&E), Masson's trichrome (MT), and Brown & Brenn (B&B) staining at the apical region after 28 days of REP. Healthy tooth: advanced root development and organized pulp tissue with blood vessels and collagen, and absence of bacteria; Necrosis: intense inflammatory infiltrate, disorganized tissue, absence of collagen and presence of bacteria; 50 mg/mL DAP and CH+3 % AZI: inflammatory cells, presence of cells in a newly formed tissue, root tip area with cementum-like tissue with cells similar to cementoblasts and cementocytes, areas of collagen, and absence of bacteria. Black arrows indicate blood vessels and white arrows indicate cementoblasts/cementocytes. Red arrows indicate the presence of bacteria in B&B staining. Abbreviations: R – root tip; PL – periodontal ligament; OL – odontoblastic layer; C – new cementum-like tissue. [H&E, MT, B&B staining; 200 ×].

fate of stem cells is well-established in the literature. Studies have demonstrated that the ECM's elasticity can direct the specification of cell lineages [34,35]. The injection could potentially negatively affect the mechanical properties of chitosan hydrogels. Our findings indicated that the incorporation of AZI resulted in slight changes to the mechanical properties of the hydrogel. Previous research on AZI-laden gelatin methacryloyl fibers also reported similar observations regarding mechanical properties [36], suggesting that the hydrophobic nature of AZI might contribute to these effects. Nevertheless, these alterations are unlikely to significantly compromise the material's performance during clinical applications in endodontics.

Various medicaments, such as triple antibiotic paste (TAP), DAP, and calcium hydroxide (Ca(OH)₂), have been historically used for root canal disinfection in REPs, each with distinct drawbacks potentially hindering the revascularization process, including adverse effects on stem cell viability and growth factors release [37–39]. Chitosan, owing to its biocompatibility, biodegradability, and non-toxicity, serves as an effective carrier for these medicaments [40]. While prior studies have demonstrated CH's effectiveness as a carrier for TAP and Ca(OH)₂, their comprehensive assessment lacked critical evaluations of mechanical properties, cytocompatibility with stem cells, and *in vivo* performance [41]. Therefore, our study investigated morphological analyses of CH hydrogels, with or without AZI, revealing a porous 3D network that facilitates controlled drug release into infected root canal systems [42, 43]. The porosity of CH hydrogels, influenced by aqueous interactions and CO_2 release during crosslinking with the gelling agent of sodium hydrogen-carbonate (SHC) [10], plays a pivotal role in drug diffusion

and release kinetics, critical for achieving therapeutic concentrations within infected dental tissues [43,44]. The 3D porous network facilitates the diffusion and controlled release of the incorporated antibacterial agent, enabling its active compounds to diffuse into the environment, such as an infected root canal system [42,43]. Pore size is also critical in cell encapsulation within polymer matrices, as it directly affects the exchange of nutrients and waste products between encapsulated cells and the surrounding tissue [45]. This parameter holds particular importance in strategies aimed at pulp regeneration, given the low vascular supply available to cells in such environments (primarily through the apical opening). Stem cells from the apical papilla (SCAPs) exhibit a spindle shape and can vary in size, typically ranging from micrometers up to around 160 μm in diameter [46]. In all hydrogel formulations, pores generally exhibit dimensions larger than SCAP cells (1–160 μm), likely facilitating sufficient nutrient and oxygen access without constraining cellular function.

Regarding the morphology and structural changes of the hydrogels after drug release, we could not directly observe these alterations due to the gradual degradation of the chitosan network during the release process. The degradation, a key mechanism driving drug release, complicates the analysis of the hydrogel's post-release morphology. As the chitosan hydrogel undergoes hydrolysis and structural breakdown, its network progressively disintegrates, making it challenging to capture distinct morphological features after the drug has been fully released [47]. This simultaneous degradation and release process is a well-recognized limitation in studying biodegradable hydrogels, where morphological changes are inherently intertwined with the degradation
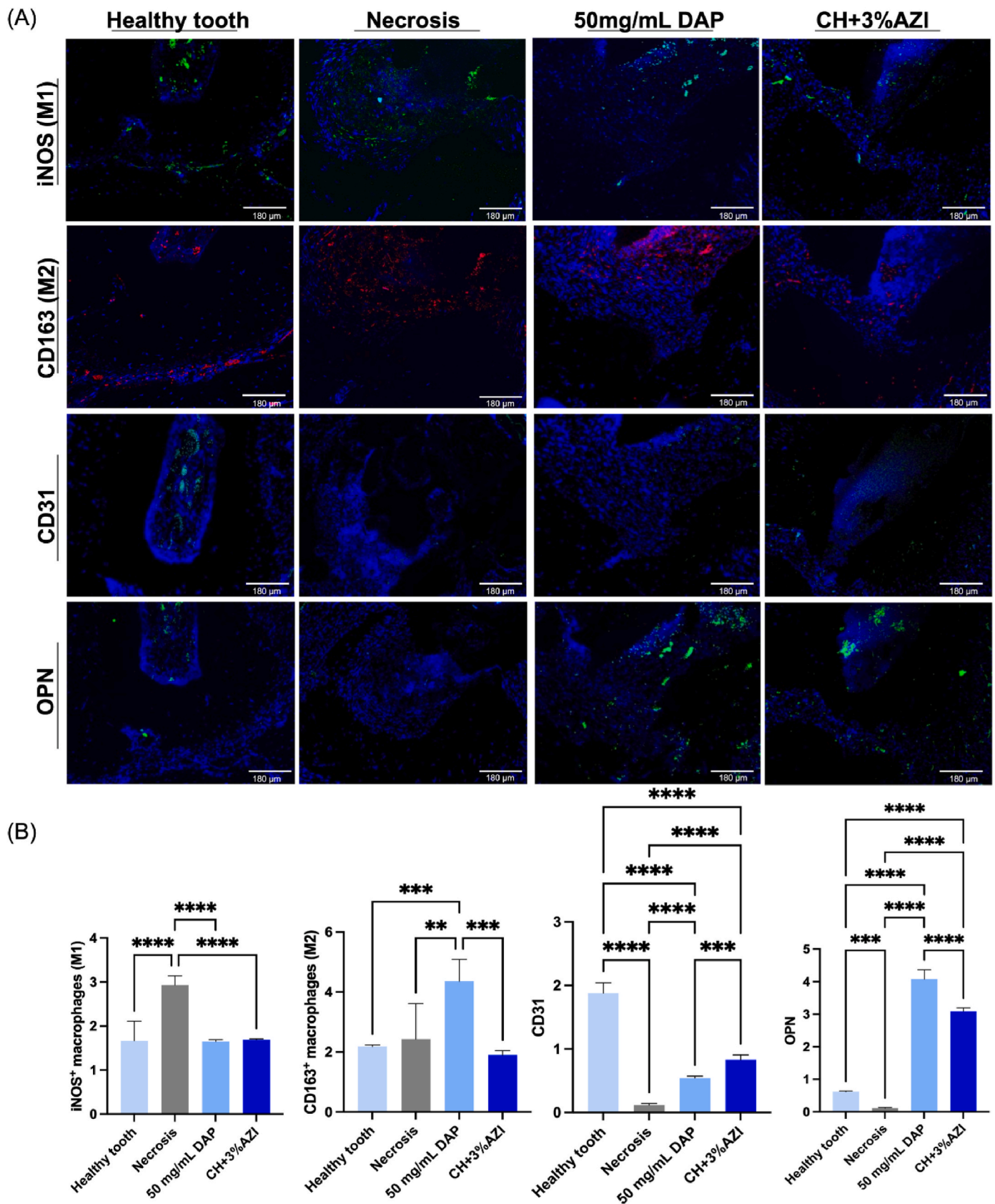
Fig. 10. Representative immunofluorescence images of iNOS (green, an M1 macrophage marker), CD163 (red, an M2 macrophage marker), CD31 (green, an endothelial marker), and OPN (green, a mineralization marker) stained cells in the apical region of the mesial root of upper first molars of rats after 28 days of REP. [Immunofluorescence staining; 100 ×]. (B) Quantification of M1-, M2-, CD31$^-$, and OPN-positive cells. *Asterisk indicates the significant difference between groups (one-way ANOVA followed by Tukey's test; **$p < 0.05$, ***$p < 0.005$, ****$p < 0.0001$).

dynamics. Consequently, detailed characterization of the hydrogel structure after drug release requires further investigation. It may necessitate using real-time techniques that can track both degradation and structural evolution.

Controlled drug release from CH hydrogels significantly impacts bioavailability and cytotoxicity profiles [48,49]. Hertwig's epithelial root sheath (HERS) and the apical papilla contribute to root canal development through epithelial-mesenchymal interactions [50]. SCAPs from apical papilla represent a promising cell source for REPs due to their proximity to tooth apices and enhanced capacity for proliferation and odontogenic differentiation compared to dental pulp stem cells (DPSCs) [51–53]. The SCAPs and some epithelial cells remain viable even in apical periodontitis, emphasizing their potential utility in REPs [50,53,54]. Therefore, determining a safe AZI concentration that demonstrates effective antimicrobial action against endodontic infections is crucial for optimizing disinfection strategies. This study revealed dose-dependent cytotoxic effects over 21 days, with lower AZI concentrations exhibiting reduced toxicity to SCAPs, possibly due to decreased drug concentration and AZI's immunomodulatory effects. These findings suggest that lower AZI concentrations provide a favorable environment for cell viability and growth [14,36].

Effective root canal disinfection is pivotal for successful REPs, especially considering microbial penetration in dentinal tubules, which is more pronounced in younger teeth due to smaller tubular dimensions [4]. CH's antimicrobial properties stem from the interaction of positively charged NH3+ groups in glucosamine with negatively charged bacterial surfaces, causing bacterial leakage and disrupting vital functions [55]. Additionally, AZI's dual-base structure facilitates its effective transport into various cells, where it binds to the bacterial 23S rRNA, thereby inhibiting protein synthesis and controlling bacterial infections [56]. Although an isolated AZI extract was not used as a control, the antibacterial findings demonstrated its efficacy, as concentrations of 3 % and 5 % AZI outperformed 0.12 % CHX and pure CH against endodontic bacteria, including *An*, commonly found in necrotic and infected immature teeth [57]. Thus, the inclusion of pure CH hydrogel, alongside CHX, as controls in the antibacterial assays allowed for the determination of AZI's influence on the zones of inhibition against the evaluated bacterial strains. Additionally, a notable reduction in the 7-day-old *Ef* biofilm was observed with both AZI-laden hydrogels (3 and 5 %) compared to a lower concentration of DAP (5 mg/mL), typically recommended for use in regenerative endodontic procedures according to current guidelines [24].

Based on these findings and considering the cytocompatibility results along with the similar antibacterial performance between both AZI concentrations, a 3 % AZI-laden CH hydrogel was selected for *in vivo* testing as an intracanal dressing in necrotic molars of rats with periapical disease. Hence, after the promising *in vitro* results of 3 % AZI incorporated into the CH hydrogel, an orthotopic model of REPs using necrotic immature rat molars was used. Early research on REPs has shown that evoked bleeding from the root apex can stimulate new tissue formation within the pulpotomized root canal space [58,59]. Importantly, factors such as the severity of the inflammatory response, the types of disinfectants used, and the presence of residual bacteria can significantly influence the healing process following REPs [60]. The present study demonstrated that using an injectable CH hydrogel with 3 % AZI effectively controlled infection, promoted increased root thickness by depositing new cementum-like tissue, and significantly reduced the volume of periapical lesions. These findings were accompanied by notable collagen fiber formation in the periapical region and its ingrowth into the root canal space post-induced bleeding, indicating a faster repair in the treated groups. However, further studies could focus on improving the biological properties of the hydrogels, such as their interaction with various cell types, including stem cells or osteoblasts, to promote tissue regeneration.

To investigate the immunomodulatory potential of the developed CH hydrogel loaded with 3 % AZI, immunofluorescence analysis was conducted for M1 (proinflammatory) and M2 (anti-inflammatory) macrophages. These cells play a crucial role in the inflammatory scenario, interacting with local stem cells, and the tissue regeneration process is characterized by the transition from M1 to M2 phenotype [61]. The results show a significant reduction in the M1 population in both treated groups compared to untreated molars with pulp necrosis and apical periodontitis. M2 macrophages in the necrosis group may indicate the host's attempt to suppress inflammation and promote tissue repair [62]. An increase in the levels of M2 macrophages was observed in the 50 mg/mL DAP group compared to the other groups. The synergistic anti-inflammatory effects of metronidazole combined with ciprofloxacin have already been demonstrated in an *in vitro* study and possibly explained by increased interleukin (IL)-10 production [63].

Osteopontin (OPN), a mineralization marker assessed in this study, is a crucial non-collagenous protein abundantly expressed in the bone matrix, playing a vital role in various biological processes such as cell adhesion, migration, and biomineralization [60,64]. In this *in vivo* study, both experimental groups showed increased OPN expression compared to the untreated groups. The significant formation of new cementum tissue at the root tip is likely associated with elevated OPN expression in these experimental groups [65,66]. A deficiency of this protein can negatively impact the development and mineralization of dentin and alveolar bone, especially in the early stages [67].

Regarding root development, a prior meta-analysis demonstrated the effectiveness of antibiotic pastes in enhancing apical repair and root lengthening, particularly by increasing dentin wall thickness [68]. The results above corroborate the findings of the present *in vivo* investigation. In addition to the increased mineralized tissue formation in the treatment groups, the injectable CH+3%AZI group exhibited enhanced angiogenesis, characterized by a significant presence of CD31-positive vessels compared to the 50 mg/mL DAP group and the necrosis group. Consistent with these histological findings, a prior *in vivo* evaluation of necrotic immature dog teeth demonstrated a significant resolution of periapical lesions, accompanied by increased root maturation and apical closure. These findings were observed in necrotic immature teeth with periapical lesions, showing continued root formation with or without the use of chitosan scaffolds and evoked bleeding [18]. These results further support the vitality and resilience of SCAP and HERS cells, even in the presence of bacterial infection and periapical disease [18,50]. Restoration of pulp tissue rich in vascular-like structures is critical for revitalizing tooth health and ensuring the long-term survival of regenerated tissue, thereby improving the retention and development of treated teeth within the oral cavity. The vascularization process involves intricate interactions among cells, soluble factors, and components of the ECM. Previous investigations [69,70] have highlighted the CH hydrogel's ability to heighten the expression of endothelial cell surface markers like CD31, suggesting their increased angiogenic potential, as seen in this study, and its potential therapeutic approach for creating a suitable environment to treat immature teeth with pulp necrosis.

This study successfully developed an injectable, in situ-gelling AZI-laden hydrogel for disinfection procedures in REPs. In addition to facilitating clinical application, the hydrogel demonstrated a 3D porous network with interconnected pores, notable mechanical and antibacterial properties even at low concentrations of AZI, and low cytotoxicity due to its controlled antibiotic release, potentially extending its application to conventional root canal treatments. Furthermore, the orthotopic animal model used in this investigation confirmed the hydrogel's ability to support tissue repair and continued root development in necrotic immature teeth by controlling infection, demonstrating angiogenic potential, and reducing inflammation. Despite these promising results, further evaluation of the hydrogel's degradation profile would provide valuable insights into its controlled drug release properties and solubility. Moreover, considering the impact of complex microbiota on the success of endodontic treatment, a multi-species biofilm evaluation could offer robust evidence of its antibacterial performance *in vivo*. Additionally, studying the release of bioactive molecules within the root

canal could enhance our understanding of whether this novel material influences the liberation of bioactive molecules from dentin, as this process is highly dependent on the synergistic effects of the irrigating solution and intracanal medications used during REPs [71]. Lastly, analyzing proliferating cell nuclear antigen-positive cells would be beneficial for indicating tissue proliferation, which is crucial for interpreting the histological outcomes observed in this study.

5. Conclusions

Our findings underscore the potential of an injectable thermosensitive CH-based hydrogel supplemented with 3 % AZI as an intracanal medication in REPs. Its ease of application and favorable safety profile offer promising prospects for effective root canal disinfection and tissue regeneration. As the first study evaluating this novel medication for REPs, further investigations are recommended to assess its antibacterial efficacy against multi-species biofilms. Long-term clinical studies are also necessary to evaluate its applicability and efficacy in enhancing REPs outcomes.

CRediT authorship contribution statement

Alexandre Henrique dos Reis-Prado: Writing – original draft, Methodology, Investigation, Formal analysis, Data curation. **Maedeh Rahimnejad:** Writing – original draft, Methodology, Investigation, Formal analysis, Data curation, Conceptualization. **Renan Dal-Fabbro:** Writing – original draft, Methodology, Investigation, Formal analysis. **Priscila Toninatto Alves de Toledo:** Writing – original draft, Investigation, Formal analysis. **Caroline Anselmi:** Writing – original draft, Methodology, Formal analysis. **Pedro Henrique Chaves de Oliveira:** Writing – original draft, Investigation, Formal analysis. **J. Christopher Fenno:** Writing – review & editing, Resources, Formal analysis. **Luciano Tavares Angelo Cintra:** Writing – review & editing, Resources, Formal analysis. **Francine Benetti:** Writing – review & editing, Supervision, Resources, Project administration, Investigation, Formal analysis. **Marco C. Bottino:** Writing – review & editing, Validation, Supervision, Resources, Project administration, Investigation, Funding acquisition, Conceptualization.

Data availability statement

Data can be provided upon reasonable request.

Ethics approval and consent to participate

Not applicable.

Funding

Declaration of competing interest

The authors declare no competing interests.

Acknowledgments

Abbreviations:

An - Actinomyces naeslundii; ATR - attenuated total reflectance mode; AZI – azithromycin; BHI - brain heart infusion; B&B – Brown and Breen; BGP - β-Glycerophosphate disodium salt hydrate; C – carbon; °C- Celcius; Ca(OH)₂ - calcium hydroxide; CH – chitosan, CFU - colony forming unit; CHX – chlorhexidine; CO_2 – carbon dioxide; DAP – double antibiotic paste; DPSCs – dental pulp stem cells; EDTA - ethylenediaminetetraacetic acid; ECM - extracellular matrix; *Ef – Enterococcus faecalis*; EDS - energy-dispersive X-ray spectroscopy; *Fn – Fusobacterium nucleatum*, FTIR - Fourier-transform infrared spectroscopy spectra; FBS – fetal bovine serum; H – hydrogen; H&E – hematoxylin and eosin; HCl - hydrochloric acid; IL – interleukin; iNOS - inducible nitric oxide synthase; LVE - linear viscoelastic region; MT – Masson's trichome; N – nitrogen; NaOCl – sodium hypochlorite; PBS - phosphate-buffered saline; PP - parallel plates; O – oxygen; OPN – osteopontin; REPs - regenerative endodontic procedures; ROI – region of interest; RT – room temperature; SCAPs - stem cells of apical papilla; SD – standard deviation; SHC - sodium hydrogen carbonate; SEM - scanning electron microscopy; TAP – triple antibiotic paste; 3D – tridimensional.

Appendix A. Supplementary data

Supplementary data to this article can be found online at https://doi.org/10.1016/j.bioactmat.2024.12.026.

References

[1] S. Kim, et al., Regenerative endodontics: a comprehensive review, Int. Endod. J. 51 (12) (2018) 1367–1388.
[2] X. Wei, et al., Expert consensus on regenerative endodontic procedures, Int. J. Oral Sci. 14 (1) (2022) 55.
[3] A.H. dos Reis-Prado, et al., Influence of ethylenediaminetetraacetic acid irrigation on the regenerative endodontic procedure in an immature rat molar model, Int. Endod. J. 56 (1) (2023) 69–79.
[4] P. Verma, et al., Effect of residual bacteria on the outcome of pulp regeneration in vivo, Journal of dental research 96 (1) (2017) 100–106.
[5] F.P. Hatipoğlu, et al., Attitude and practice of regenerative endodontic procedures among endodontists and paediatric dentists: a multinational survey from 13 countries, Int. J. Paediatr. Dent. 33 (5) (2023) 521–534.
[6] J.S. Ribeiro, et al., Antimicrobial therapeutics in regenerative endodontics: a scoping review, J. Endod. 46 (9) (2020) S115–S127.
[7] P. Taweewattanapaisan, et al., The effects of EDTA on blood clot in regenerative endodontic procedures, J. Endod. 45 (3) (2019) 281–286.
[8] H. Liu, et al., Biomaterial scaffolds for clinical procedures in endodontic regeneration, Bioact. Mater. 12 (2022) 257–277.
[9] G. Tang, et al., Recent advances of chitosan-based injectable hydrogels for bone and dental tissue regeneration, Front. Bioeng. Biotechnol. 8 (2020) 587658.
[10] E. Assaad, M. Maire, S. Lerouge, Injectable thermosensitive chitosan hydrogels with controlled gelation kinetics and enhanced mechanical resistance, Carbohydrate polymers 130 (2015) 87–96.
[11] M. Rahimnejad, Thermosensitive Chitosan-Based Hydrogels for Extrusion-Based Bioprinting and Injectable Scaffold for Articular Tissue Engineering, 2022.
[12] J. Segura-Egea, et al., Antibiotics in endodontics: a review, Int. Endod. J. 50 (12) (2017) 1169–1184.
[13] A. Firth, P. Prathapan, Azithromycin: the first broad-spectrum therapeutic, Eur. J. Med. Chem. 207 (2020) 112739.
[14] A.C. Andrada, et al., Immunomodulation mediated by azithromycin in experimental periapical inflammation, J. Endod. 46 (11) (2020) 1648–1654.
[15] N. Meschi, P.J. Palma, D. Cabanillas-Balsera, Effectiveness of revitalization in treating apical periodontitis: a systematic review and meta-analysis, Int. Endod. J. 56 (2023) 510–532.
[16] A. Youssef, et al., Regenerative endodontic procedures for the treatment of necrotic mature teeth: a preliminary randomized clinical trial, Int. Endod. J. 55 (4) (2022) 334–346.
[17] A. Al-Qudah, et al., Outcome of regenerative endodontic procedures in nonvital immature permanent teeth using 2 intracanal medications: a prospective randomized clinical study, J. Endod. 49 (7) (2023) 776–785.

[18] P.J. Palma, et al., Histologic evaluation of regenerative endodontic procedures with the use of chitosan scaffolds in immature dog teeth with apical periodontitis, J. Endod. 43 (8) (2017) 1279–1287.

[19] M. Leveque, et al., Next generation antibacterial strategies for regenerative endodontic procedures: a scoping review, Int. Endod. J. 57 (7) (2024) 804–814.

[20] M.S. Moreira, et al., Physical and biological properties of a chitosan hydrogel scaffold associated to photobiomodulation therapy for dental pulp regeneration: an in vitro and in vivo study, BioMed Res. Int. 2021 (1) (2021) 6684667.

[21] M. Rahimnejad, et al., A rheological approach to assess the printability of thermosensitive chitosan-based biomaterial inks, Biomedical Materials 16 (1) (2020) 015003.

[22] J.S. Ribeiro, et al., Photocrosslinkable methacrylated gelatin hydrogel as a cell-friendly injectable delivery system for chlorhexidine in regenerative endodontics, Dent. Mater. 38 (9) (2022) 1507–1517.

[23] A. Silverberg, et al., Metronidazole-laden silk fibroin methacrylated scaffolds for managing periapical lesions, Odontology (2024) 1–14.

[24] Chicago: American Association of Endodontists: Chicago: American Association of Endodontists. Available at: https://www.aae.org/specialty/wp-content/uploads/sites/2/2021/08/ClinicalConsiderationsApprovedByREC062921.pdf).

[25] R.K. Scarparo, et al., Intracanal delivery of Resolvin E1 controls inflammation in necrotic immature rat teeth, J. Endod. 40 (5) (2014) 678–682.

[26] I. Bracks, et al., Effect of ethylenediaminetetraacetic acid irrigation on immune-inflammatory response in teeth submitted to regenerative endodontic therapy, Int. Endod. J. 52 (10) (2019) 1457–1465.

[27] C.F.B. Wolle, et al., Effects of the antioxidant agent tempol on periapical lesions in rats with doxorubicin-induced cardiomyopathy, J. Endod. 38 (2) (2012) 191–195.

[28] R.C.S. Barcelos, et al., Apical periodontitis induces changes on oxidative stress parameters and increases Na+/K+-ATPase activity in adult rats, Arch. Oral Biol. 118 (2020) 104849.

[29] H.H. Winter, F. Chambon, Analysis of linear viscoelasticity of a crosslinking polymer at the gel point, Journal of rheology 30 (2) (1986) 367–382.

[30] A.H. dos Reis-Prado, et al., Top 100 most-cited scientific articles in regenerative endodontics 2019–2023: a bibliometric analysis, Int. Endod. J. (2024).

[31] V.O. Fasiku, et al., Chitosan-based hydrogel for the dual delivery of antimicrobial agents against bacterial methicillin-resistant Staphylococcus aureus biofilm-infected wounds, ACS Omega 6 (34) (2021) 21994–22010.

[32] M. Rahimnejad, et al., Injectable cell-laden hybrid bioactive scaffold containing bioactive glass microspheres, J. Biomed. Mater. Res. 111 (7) (2023) 1031–1043.

[33] C. Yan, et al., Injectable solid peptide hydrogel as a cell carrier: effects of shear flow on hydrogels and cell payload, Langmuir 28 (14) (2012) 6076–6087.

[34] A.J. Engler, et al., Matrix elasticity directs stem cell lineage specification, Cell 126 (4) (2006) 677–689.

[35] E. Prateeptongkum, The Influence of Substrate Stiffness on the Osteogenic Differentiation of Stem-And Progenitor Cells from Dental Tissue, 2015.

[36] A.A. Ayoub, et al., Electrospun azithromycin-laden gelatin methacryloyl fibers for endodontic infection control, Int. J. Mol. Sci. 23 (22) (2022) 13761.

[37] R.I. Althumairy, F.B. Teixeira, A. Diogenes, Effect of dentin conditioning with intracanal medicaments on survival of stem cells of apical papilla, J. Endod. 40 (4) (2014) 521–525.

[38] N. Labban, et al., The direct cytotoxic effects of medicaments used in endodontic regeneration on human dental pulp cells, Dent. Traumatol. 30 (6) (2014) 429–434.

[39] K.M. Galler, et al., Influence of root canal disinfectants on growth factor release from dentin, J. Endod. 41 (3) (2015) 363–368.

[40] J. Li, et al., Chitosan-based nanomaterials for drug delivery, Molecules 23 (10) (2018) 2661.

[41] J. Shaik, et al., Comparative evaluation of antimicrobial efficacy of triple antibiotic paste and calcium hydroxide using chitosan as carrier against Candida albicans and Enterococcus faecalis: an: in vitro: study, Journal of Conservative Dentistry and Endodontics 17 (4) (2014) 335–339.

[42] S. Khan, et al., Insight into hydrogels, Des. Monomers Polym. 19 (5) (2016) 456–478.

[43] N. Raina, et al., Drug delivery strategies and biomedical significance of hydrogels: translational considerations, Pharmaceutics 14 (3) (2022) 574.

[44] R. Dal-Fabbro, et al., Injectable methacrylated gelatin hydrogel for safe sodium hypochlorite delivery in endodontics, Gels 9 (11) (2023) 897.

[45] L. Lambricht, et al., The type and composition of alginate and hyaluronic-based hydrogels influence the viability of stem cells of the apical papilla, Dent. Mater. 30 (12) (2014) e349–e361.

[46] M. Mavinga, et al., The journey of SCAPs (stem cells from apical papilla), from their native tissue to grafting: impact of oxygen concentration, Cells 11 (24) (2022) 4098.

[47] H.D. Han, et al., Preparation and biodegradation of thermosensitive chitosan hydrogel as a function of pH and temperature, Macromol. Res. 12 (2004) 507–511.

[48] H. Hamedi, et al., Chitosan based hydrogels and their applications for drug delivery in wound dressings: a review, Carbohydrate polymers 199 (2018) 445–460.

[49] J. Hu, et al., Visible light crosslinkable chitosan hydrogels for tissue engineering, Acta Biomater. 8 (5) (2012) 1730–1738.

[50] P.J. Palma, et al., Does apical papilla survive and develop in apical periodontitis presence after regenerative endodontic procedures? Appl. Sci. 9 (19) (2019) 3942.

[51] D.B. Sequeira, et al., Regeneration of pulp-dentin complex using human stem cells of the apical papilla: in vivo interaction with two bioactive materials, Clin. Oral Invest. 25 (2021) 5317–5329.

[52] Q. Liu, Y. Gao, J. He, Stem cells from the apical papilla (SCAPs): past, present, prospects, and challenges, Biomedicines 11 (7) (2023) 2047.

[53] A. Digka, D. Sakka, K. Lyroudia, Histological assessment of human regenerative endodontic procedures (REP) of immature permanent teeth with necrotic pulp/apical periodontitis: a systematic review, Aust. Endod. J. 46 (1) (2020) 140–153.

[54] P.C.T. Duarte, et al., Histopathological condition of the remaining tissues after endodontic infection of rat immature teeth, J. Endod. 40 (4) (2014) 538–542.

[55] S.M. Mawazi, et al., Recent applications of chitosan and its derivatives in antibacterial, anticancer, wound healing, and tissue engineering fields, Polymers 16 (10) (2024) 1351.

[56] P.A. Moore, Dental therapeutic indications for the newer long-acting macrolide antibiotics, The Journal of the American Dental Association 130 (9) (1999) 1341–1343.

[57] A.F. Fouad, Microbiological aspects of traumatic injuries, J. Endod. 45 (12) (2019) S39–S48.

[58] B.N. Östby, The role of the blood clot in endodontic therapy an experimental histologic study, Acta Odontol. Scand. 19 (3–4) (1961) 323–353.

[59] B. Nygaard-Östby, O. Hjortdal, Tissue formation in the root canal following pulp removal, Eur. J. Oral Sci. 79 (3) (1971) 333–349.

[60] N. Edanami, et al., Impact of remnant healthy pulp and apical tissue on outcomes after simulated regenerative endodontic procedure in rat molars, Sci. Rep. 10 (1) (2020) 20967.

[61] B. Gu, et al., Macrophage populations show an M1-to-M2 transition in an experimental model of coronal pulp tissue engineering with mesenchymal stem cells, Int. Endod. J. 52 (4) (2019) 504–514.

[62] P.J. Murray, T.A. Wynn, Protective and pathogenic functions of macrophage subsets, Nat. Rev. Immunol. 11 (11) (2011) 723–737.

[63] E.E. Tan, et al., Antibiotics used in regenerative endodontics modify immune response of macrophages to bacterial infection, J. Endod. 45 (11) (2019) 1349–1356.

[64] M. McKee, A. Nanci, Osteopontin at mineralized tissue interfaces in bone, teeth, and osseointegrated implants: ultrastructural distribution and implications for mineralized tissue formation, turnover, and repair, Microsc. Res. Tech. 33 (2) (1996) 141–164.

[65] D. Chaikiawkeaw, et al., Osteopontin induces osteogenic differentiation by human periodontal ligament cells via calcium binding domain–ALK-1 interaction, J. Periodontol. 93 (2) (2022) e13–e23.

[66] B. Foster, et al., Deficiency in acellular cementum and periodontal attachment in bsp null mice, Journal of dental research 92 (2) (2013) 166–172.

[67] B. Foster, et al., Osteopontin regulates dentin and alveolar bone development and mineralization, Bone 107 (2018) 196–207.

[68] V. Báez, et al., Meta-analysis of regenerative endodontics outcomes with antibiotics pastes and calcium hydroxide. The apex of the iceberg, Journal of Oral Biology and Craniofacial Research 12 (1) (2022) 90–98.

[69] Y. Yang, et al., Mussel-inspired adhesive antioxidant antibacterial hemostatic composite hydrogel wound dressing via photo-polymerization for infected skin wound healing, Bioact. Mater. 8 (2022) 341–354.

[70] M. Hao, et al., Chitosan/sodium alginate/velvet antler blood peptides hydrogel promotes diabetic wound healing via regulating angiogenesis, inflammatory response and skin flora, J. Inflamm. Res. (2022) 4921–4938.

[71] G. Bilvinaite, et al., Effect of calcium silicate-based intracanal medicament and calcium hydroxide on growth factor TGF-β1 release from root canal dentine, J. Funct. Biomater. 15 (6) (2024) 139.